Theoretical Analysis of the No-Slip Boundary Condition Enforcement in SPH Methods

Fabricio Maciá,[1] Matteo Antuono,[2] Leo M. González[1]
and Andrea Colagrossi[2,3]

[1]*Naval Architecture Dept. (ETSIN), Technical University of Madrid (UPM), 28040 Madrid, Spain*
[2]*CNR-INSEAN (The Italian Ship Model Basin), Via di Vallerano 139, 00128 Roma, Italy*
[3]*Centre of Excellence for Ship and Ocean Structures (CESOS), NTNU, Trondheim, Norway*

The aim of the present work is to provide an in-depth analysis of the most representative mirroring techniques used in SPH to enforce boundary conditions (BC) along solid profiles. We specifically refer to dummy particles, ghost particles, and Takeda et al. [Prog. Theor. Phys. **92** (1994), 939] boundary integrals. The analysis has been carried out by studying the convergence of the first- and second-order differential operators as the smoothing length (that is, the characteristic length on which relies the SPH interpolation) decreases. These differential operators are of fundamental importance for the computation of the viscous drag and the viscous/diffusive terms in the momentum and energy equations. It has been proved that close to the boundaries some of the mirroring techniques leads to intrinsic inaccuracies in the convergence of the differential operators. A consistent formulation has been derived starting from Takeda et al. boundary integrals (see the above reference). This original formulation allows implementing no-slip boundary conditions consistently in many practical applications as viscous flows and diffusion problems.

Subject Index: 024

§1. Introduction

The Smoothed Particle Hydrodynamics scheme (hereinafter SPH) is a Lagrangian model based on a smoothing of the spatial differential operators of the fluid-dynamics equations and on their subsequent discretization through a finite number of fluid particles. The smoothing procedure (which is made at the continuum level) is performed by using a weight function (also called kernel function) with a compact support whose characteristic length is the smoothing length h. After the smoothed equations are discretized through fluid particles, the resolution of the discrete SPH scheme is a function of both the smoothing length and the mean particle distance dx. In this framework, the (continuous) equations of the fluid-dynamics should be recovered as both h and dx/h tend simultaneously to zero.[4]

The SPH simulations in engineering involve usually solid boundary conditions (BC) for the velocity field and Dirichlet and Neumann type BC for other fields as, for instance, the temperature. In the SPH framework, these conditions are tackled in a number of ways: by using boundary forces-type models;[5] by modifying the structure of the kernel in the neighborhood of the boundaries;[6] by creating virtual

particles inside the solid boundary domain through mirroring techniques. This latter approach is the main focus of the present work.

The need for virtual particles arises mainly from the incompleteness of the kernel close to the boundary. Creating those particles produces an immersion of the solid boundary into a complete kernel region. Note that Peskin's[7] immersed boundary method (IBM) can be seen as a precedent of these techniques. Differential operators are then evaluated close to the boundary using these virtual particles, whose properties are obtained from the fluid region through mirroring techniques.

Unfortunately, the consistency of these operators at the boundary has not received much attention in the SPH literature. The present work provides a detailed insight on this topic by studying the convergence of the SPH smoothing and differential operators when the different mirroring techniques are used. Similarly to the work of Colagrossi et al.[8] who discussed the influence of the truncation of differential operators close to a free surface, the present analysis has been performed at the continuum. Incidentally, we underline that at the discrete level the accuracy of the different approximations of the viscous terms has been widely discussed.[6],[9]–[13] Notwithstanding that, our analysis shows some new and important results. First, we prove that intrinsic inaccuracies arise in the evaluation of the SPH differential operators and, for some mirroring techniques, the occurrence of singularities is observed. This problem is also relevant at the discrete level. In Colagrossi et al.[14] and in Souto et al.,[15] the consistency of the mirroring techniques was studied by performing a series of numerical test cases. That analysis clearly proved the existence of incongruities in the evaluation of the viscous term close to the solid boundaries. Then, starting from the work of Takeda et al.,[1] we derived a novel consistent mirroring technique. This is accurate up to second-order differential operators and, therefore, proves to be appropriate for flows in which diffusive/dissipative effects play a relevant role.

The paper is organized as follows: first, the SPH formalism is presented and the consistency of the first- and second-order differential operators far from the boundaries is summarized. The properties of these operators are, then, explored when acting on fields defined close to a boundary for a class of mirroring techniques widely used in practical applications. Intrinsic inaccuracies are found in the computation of these operators close to the boundaries and, for some flows and mirroring techniques combinations, the occurrence of singularities is detected. Finally, the original consistent formulation is presented and some numerical test cases are performed in order to prove the relevance of the theoretical findings in actual applications.

§2. Continuous SPH approximation of differential operators

Before proceeding to the analysis, we briefly recall the principal results about the consistency of the continuous SPH formulation without boundaries. The fluid domain is $\Omega = \mathbb{R}^d$ and, therefore, its boundary is $\partial\Omega = \emptyset$.

Let $W(\boldsymbol{x}; h)$ be a function depending on $h > 0$ defined by

$$W(\boldsymbol{x}; h) := \frac{1}{h^d}\tilde{W}\left(\left|\frac{\boldsymbol{x}}{h}\right|\right), \qquad (2\cdot1)$$

where $\tilde{W} : \mathbb{R} \rightarrow \mathbb{R}$ is a *nonnegative differentiable function* such that:

$$1 = \int_{\mathbb{R}^d} \tilde{W}\left(|\boldsymbol{x}|\right) d\boldsymbol{x} = \omega_d \int_0^\infty \tilde{W}\left(r\right) r^{d-1} dr, \tag{2·2}$$

and the constant ω_d represents the volume of the unit sphere in $\mathbb{R}^d$. We also assume that the function

$$F\left(r\right) := -\frac{1}{r}\tilde{W}'\left(r\right), \tag{2·3}$$

is *bounded and nonnegative* for $r \geq 0$ and that:

$$\sup_{r>0} r^\alpha \tilde{W}\left(r\right), \quad \sup_{r>0} r^\alpha \tilde{W}'\left(r\right), \qquad \text{are finite for any } \alpha > 0. \tag{2·4}$$

This amounts to saying that $\tilde{W}$ and its derivative decay at infinity faster than any polynomial function. This condition is satisfied if, for instance, $\tilde{W}$ is a Gaussian function or has bounded support. Note that

$$\nabla_{\boldsymbol{x}} W\left(\boldsymbol{x}; h\right) = -\frac{1}{h^{d+2}} F\left(\frac{|\boldsymbol{x}|}{h}\right) \boldsymbol{x}. \tag{2·5}$$

In the following we denote by $u\left(\boldsymbol{x}\right)$ a smooth scalar field on $\mathbb{R}^d$.

- The continuous SPH approximation of the velocity field u through the kernel W is defined as:

$$\langle u \rangle\left(\boldsymbol{x}\right) := \int_{\mathbb{R}^d} u\left(\boldsymbol{x}'\right) W\left(\boldsymbol{x} - \boldsymbol{x}'; h\right) d\boldsymbol{x}'. \tag{2·6}$$

This expression implies (see, for instance, Colagrossi & Landrini[16]):

$$\langle u \rangle\left(\boldsymbol{x}\right) = u\left(\boldsymbol{x}\right) + \mathcal{O}(h^2). \tag{2·7}$$

- Partial derivatives $\partial_{x_k} u$ are approximated by:

$$\langle \partial_{x_k} u \rangle\left(\boldsymbol{x}\right) := \int_{\mathbb{R}^d} u\left(\boldsymbol{x}'\right) \partial_{x_k} W\left(\boldsymbol{x} - \boldsymbol{x}'; h\right) d\boldsymbol{x}'. \tag{2·8}$$

This formula is equivalent to (2·6) since the hypotheses made on the kernel ensure that:

$$\langle \partial_{x_k} u \rangle\left(\boldsymbol{x}\right) = \partial_{x_k} \langle u \rangle\left(\boldsymbol{x}\right) = -\int_{\mathbb{R}^d} u\left(\boldsymbol{x}'\right) \partial_{x_k'} W\left(\boldsymbol{x} - \boldsymbol{x}'; h\right) d\boldsymbol{x}$$

$$= \int_{\mathbb{R}^d} \partial_{x_k'} u\left(\boldsymbol{x}'\right) W\left(\boldsymbol{x} - \boldsymbol{x}'; h\right) d\boldsymbol{x},$$

by integration by parts. However, note that (2·8) makes sense even if the partial derivatives of u are not well-defined. It follows (see, for instance, Hu & Adams[17]) that:

$$\langle \partial_{x_k} u \rangle\left(\boldsymbol{x}\right) = \partial_{x_k} u + \mathcal{O}\left(h^2\right). \tag{2·9}$$

- The approximation $\langle \Delta u \rangle$ for the Laplacian of a function is seldom used. Instead of it, the following formula due to Morris et al. (M)[2] and Español et al.[18] is preferred in the SPH framework:

$$\langle \Delta u \rangle_{\mathrm{M}} (\boldsymbol{x}) := 2 \int_{\mathbb{R}^d} \frac{(\boldsymbol{x}' - \boldsymbol{x}) \cdot \nabla_{\boldsymbol{x}} W (\boldsymbol{x}' - \boldsymbol{x}; h)}{|\boldsymbol{x}' - \boldsymbol{x}|^2} \left[u(\boldsymbol{x}') - u(\boldsymbol{x}) \right] d\boldsymbol{x}'. \quad (2\cdot10)$$

As proved in Español & Revenga,[18] it follows:

$$\langle \Delta u \rangle_{\mathrm{M}} (\boldsymbol{x}) = \Delta u(\boldsymbol{x}) + \mathcal{O}(h^2). \quad (2\cdot11)$$

Again, note that no *a priori* assumptions on the smoothness of u have to be made in order to define $\langle \Delta u \rangle_{\mathrm{M}}$.

- Finally, let us recall the approximation of the Laplacian of the velocity field $\boldsymbol{u} := (u_1, ..., u_d)$ introduced by Monaghan-Cleary-Gingold (MCG)[3] for incompressible flows:

$$\langle \Delta \boldsymbol{u} \rangle_{\mathrm{MCG}} (\boldsymbol{x}) = 2(d+2) \int_{\mathbb{R}^d} \frac{(\boldsymbol{x}' - \boldsymbol{x}) \cdot (\boldsymbol{u}(\boldsymbol{x}') - \boldsymbol{u}(\boldsymbol{x}))}{|\boldsymbol{x}' - \boldsymbol{x}|^2} \nabla_{\boldsymbol{x}} W (\boldsymbol{x}' - \boldsymbol{x}; h) \, d\boldsymbol{x}'. \quad (2\cdot12)$$

If the velocity field is unidirectional and only depends on the last variable x_d, i.e.

$$\boldsymbol{u}(\boldsymbol{x}) = (u(x_d), 0, ..., 0), \quad (2\cdot13)$$

then the field $\langle \Delta \boldsymbol{u} \rangle_{\mathrm{MCG}}$ is of the form:

$$\langle \Delta \boldsymbol{u} \rangle_{\mathrm{MCG}} = \left(\langle \Delta \boldsymbol{u} \rangle^1_{\mathrm{MCG}}, 0, ..., 0 \right), \quad (2\cdot14)$$

(for details, see identities (B·3a), (B·3b), (B·4) in Appendix B). This means that only its first component is not identically zero. Therefore, given a smooth scalar field u depending on the variable x_d, we shall make a slight abuse of notation and write

$$\langle \Delta u \rangle_{\mathrm{MCG}} := \langle \Delta \boldsymbol{u} \rangle^1_{\mathrm{MCG}}, \quad (2\cdot15)$$

where $\boldsymbol{u}$ is the velocity field defined by (2·13).

Next, we recall the consistency properties of these approximation schemes. For the sake of simplicity, we show them for functions $u(\boldsymbol{x}) = x_d^p$, $p = 0, 1, ...$ depending only on the last variable.

1. For $p = 0, 1$ the approximation $\langle u \rangle$ is exact:

$$\langle 1 \rangle = 1, \quad \langle x_d \rangle = x_d, \quad (2\cdot16)$$

while for $p \geq 2$,

$$\langle x_d^p \rangle = x_d^p + \mathcal{O}\left(h^2\right). \quad (2\cdot17)$$

2. The approximation of the partial derivative $\langle \partial_{x_d} u \rangle$ is exact for $p \leq 2$:

$$\langle \partial_{x_d} 1 \rangle = 0, \quad \langle \partial_{x_d} x_d \rangle = 1, \quad \langle \partial_{x_d} x_d^2 \rangle = 2x_d, \quad (2\cdot18)$$

while for $p \geq 3$ we have:

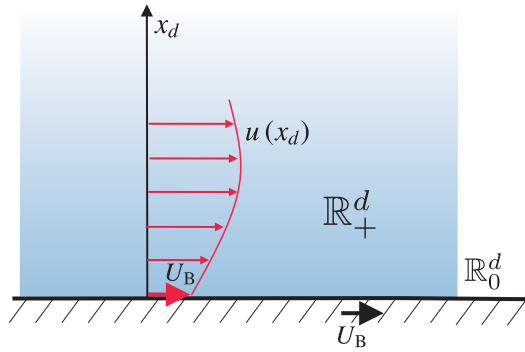$$\langle \partial_{x_d} x_d^p \rangle = p x_d^{p-1} + \mathcal{O}\left(h^2\right). \quad (2\cdot19)$$

Fig. 1.   Unidirectional vector field.

3. The approximate Laplacian is exact for polynomials of degree $p \leq 3$ (see Español & Revenga[18)]):

$$\langle \Delta 1 \rangle_{\mathrm{M}} = 0, \quad \langle \Delta x_d \rangle_{\mathrm{M}} = 0, \quad \langle \Delta x_d^2 \rangle_{\mathrm{M}} = 2, \quad \langle \Delta x_d^3 \rangle_{\mathrm{M}} = 6 x_d, \tag{2·20}$$

while for $p \geq 4$:

$$\langle \Delta x_d^p \rangle_{\mathrm{M}} = p \left(p - 1 \right) x_d^{p-2} + \mathcal{O} \left(h^2 \right). \tag{2·21}$$

4. Note that the unidirectional field (2·13) is divergence-free. Then, as proved in Hu & Adams,[17)] if $u \left(x_d \right) = x_d^p$ is a polynomial with $p \leq 3$

$$\langle \Delta x_d^p \rangle_{\mathrm{MCG}} = \langle \Delta x_d^p \rangle_{\mathrm{M}} = \Delta x_d^p = p \left(p - 1 \right) x_d^{p-2}, \tag{2·22}$$

while for $p \geq 4$

$$\langle \Delta x_d^p \rangle_{\mathrm{MCG}} = \langle \Delta x_d^p \rangle_{\mathrm{M}} + \mathcal{O} \left(h^2 \right) = p \left(p - 1 \right) x_d^{p-2} + \mathcal{O} \left(h^2 \right). \tag{2·23}$$

§3.   Analysis of the mirroring models

The most representative mirroring techniques in SPH are: rows of fixed (boundary velocity) dummy particles (U0M),[3)] ghost particles with antisymmetric mirroring (ASM)[16), 19)] and the Takeda et al.[1)] imaginary particles. For completeness, we add to these ones the symmetric mirroring technique (SSM) which is generally used to mirror the tangential velocity when free slip boundary conditions are imposed.[16)]

For the sake of simplicity, we consider unidirectional velocity fields $\boldsymbol{u} \left(\boldsymbol{x} \right)$ defined in the upper-half plane

$$\mathbb{R}_+^d := \left\{ \left(\boldsymbol{x}', x_d \right) \in \mathbb{R}^d : x_d > 0 \right\},$$

that are infinitely differentiable and that satisfy a no-slip boundary condition on

$$\mathbb{R}_0^d := \partial \mathbb{R}_+^d = \left\{ \left(\boldsymbol{x}', 0 \right) : \boldsymbol{x}' \in \mathbb{R}^{d-1} \right\}.$$

The fact that $\partial \mathbb{R}_+^d$ is a planar boundary is far form being overly restrictive. In fact, a regular solid surface can be approximated with its tangent plane in the neighborhood

of the fluid particle for $h \ll 1$. In this framework, the tangent plane can be identified with $x_d = 0$.

This class of velocity fields appear in a number of canonical problems in different physical contexts as, for instance, unidirectional incompressible fluid flow (Couette, plane Poiseuille, etc.). Note that heat conduction problems also fit this framework by replacing the velocity with the temperature field.

In general, such a velocity field has the following form (see Fig. 1):

$$\boldsymbol{u}\left(\boldsymbol{x}\right) := \left(u\left(x_d\right), 0, ..., 0\right). \tag{3·1}$$

We assume that $\boldsymbol{u}\left(\boldsymbol{x}\right)$ satisfies the boundary condition:

$$\boldsymbol{u}\left(\boldsymbol{x}', 0\right) = \left(u\left(0\right), 0, ..., 0\right) = \left(U_{\mathrm{B}}, 0, ..., 0\right),$$

where U_{B} is the boundary velocity magnitude and, close to the boundary inside the fluid domain, the component u has the form:

$$u\left(x_d\right) = U_{\mathrm{B}} + a_1 x_d + a_2 x_d^2 + ... \tag{3·2}$$

The mirroring techniques we deal with produce an extension $\overline{\boldsymbol{u}}\left(\boldsymbol{x}\right)$ of the velocity field $\boldsymbol{u}\left(\boldsymbol{x}\right)$ to the whole space $\mathbb{R}^d$. Here, we analyze the action of the continuous SPH approximation of the differential operators introduced in §2 on these mirrored (extended) velocity fields. Due to the specific form of the velocity fields, this corresponds to an extension of the scalar function $u\left(x_d\right)$, defined only of the half axis $x_d \geq 0$, to a function $\overline{u}\left(x_d\right)$ defined on the whole real line $\mathbb{R}$. The linear character of the differential operators considered here, allows us to study independently their action on each of the summands in the expansion (3·2).

All the mirroring procedures have the property that the constant profile $u\left(x_d\right) = U_{\mathrm{B}}$ extends to $\mathbb{R}^d$ as $\overline{u}\left(x_d\right) = U_{\mathrm{B}}$. Therefore, in view of the considerations made in §2 we deduce that:

$$\langle\overline{u}\rangle\left(\boldsymbol{x}', 0\right) = \overline{u}\left(0\right) = U_{\mathrm{B}},$$

and

$$\langle\partial_{x_d}\overline{u}\rangle\left(\boldsymbol{x}', 0\right) = \langle\varDelta\overline{u}\rangle_{\mathrm{M}}\left(\boldsymbol{x}', 0\right) = \langle\varDelta\overline{u}\rangle_{\mathrm{MCG}}\left(\boldsymbol{x}', 0\right) = 0.$$

Note that the mirroring techniques extend a continuous function on $\mathbb{R}_+^d$ to a continuous function on $\mathbb{R}^d$. Therefore, the SPH approximations $\langle\overline{u}\rangle$ and $\langle\partial_{x_d}\overline{u}\rangle$ to $\overline{u}$ (which is continuous) and $\partial_{x_d}\overline{u}$ (which may present discontinuities) respectively, are always smooth functions on $\mathbb{R}^d$. On the other hand, the SPH approximations to the Laplacian of $\overline{u}$, $\langle\varDelta\overline{u}\rangle_{\mathrm{M}}$ and $\langle\varDelta\overline{u}\rangle_{\mathrm{MCG}}$ are of the same order of differentiability of $\overline{u}$.

Finally, in order to lighten our writing, we introduce the following h-independent constants that will appear repeatedly in the rest of the article:

$$M_0 := \int_{\mathbb{R}^d} F\left(|\boldsymbol{y}|\right) d\boldsymbol{y}, \tag{3·3}$$

$$M_1 := \int_{\mathbb{R}_+^d} y_d F\left(|\boldsymbol{y}|\right) d\boldsymbol{y}, \tag{3·4}$$
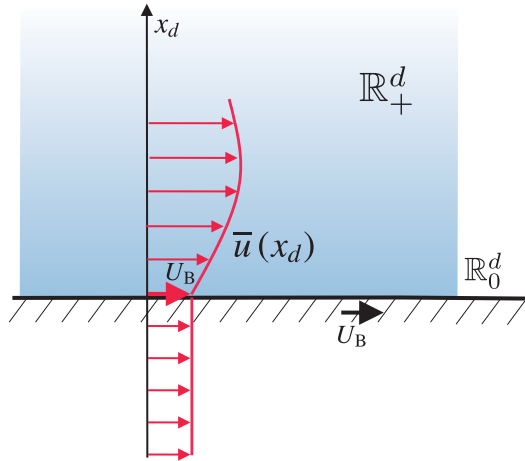
Fig. 2.   Constant extension U0M.

$$C_p := \int_{\mathbb{R}^d} |y_d|^p \, \tilde{W}\left(|\boldsymbol{y}|\right) d\boldsymbol{y}, \tag{3.5}$$

$$K_p := \int_{\mathbb{R}^d_+} \frac{y_d^p y_1^2}{|\boldsymbol{y}|^2} F\left(|\boldsymbol{y}|\right) d\boldsymbol{y}. \tag{3.6}$$

Note that $C_0 = 1$ and $K_2 = 1/2\,(d+2)$.

3.1.   *Constant extension (U0M)*

Define the constant extension of u as (see Fig. 2):

$$\overline{u}\left(\boldsymbol{x}\right) := \left\{ \begin{array}{ll} u\left(\boldsymbol{x}\right) & x_d > 0, \\ U_{\mathrm{B}} & x_d \leq 0. \end{array} \right.$$

This technique is usually referred to as the Dummy Particles (DP) method. It is simple to implement and has been used, for instance, by Monaghan[3] for modeling a transient Couette flow.

Since the function $u\left(\boldsymbol{x}\right)$ only depends on x_d, we obtain the following expression for the boundary values of the different SPH approximations:

$$\langle\overline{u}\rangle\left(\boldsymbol{x}',0\right) = \int_{\mathbb{R}^d_+} u\left(hy_d\right) \tilde{W}\left(|\boldsymbol{y}|\right) d\boldsymbol{y} + \frac{U_{\mathrm{B}}}{2}, \tag{3.7}$$

$$\langle\partial_{x_k}\overline{u}\rangle\left(\boldsymbol{x}',0\right) = \frac{1}{h}\left[\int_{\mathbb{R}^d_+} u\left(hy_d\right) y_k F\left(|\boldsymbol{y}|\right) d\boldsymbol{y} - U_{\mathrm{B}} M_1\right], \tag{3.8}$$

$$\langle\Delta\overline{u}\rangle_{\mathrm{M}}\left(\boldsymbol{x}',0\right) = \frac{2}{h^2}\left[\int_{\mathbb{R}^d_+} u\left(hy_d\right) F\left(|\boldsymbol{y}|\right) d\boldsymbol{y} - U_{\mathrm{B}}\frac{M_0}{2}\right], \tag{3.9}$$

$$\langle\Delta\overline{u}\rangle_{\mathrm{MCG}}\left(\boldsymbol{x}',0\right) = \frac{2\,(d+2)}{h^2}\left[\int_{\mathbb{R}^d_+} u\left(hy_d\right) \frac{y_1^2}{|\boldsymbol{y}|^2} F\left(|\boldsymbol{y}|\right) d\boldsymbol{y} - U_{\mathrm{B}}\frac{M_0}{2d}\right]. \tag{3.10}$$

Details on the derivation of these formulas are given in Appendix B.1. Note that $\langle \partial_{x_k} \overline{u} \rangle = 0$ if $k \neq d$.

Consider a general polynomial profile $u\left(\boldsymbol{x}\right) = U_{\mathrm{B}} + x_d^p$ with $p \geq 1$. The following expression holds:

$$\langle \overline{u} \rangle \left(\boldsymbol{x}', 0\right) = U_{\mathrm{B}} + h^p \int_{\mathbb{R}_+^d} y_d^p \tilde{W}\left(|\boldsymbol{y}|\right) d\boldsymbol{y} = U_{\mathrm{B}} + h^p \frac{C_p}{2}.$$

Using the identities (A·5), (A·6), (A·7) in the Appendix A and the fact that all differential operators are linear (and therefore, $\langle \partial_{x_d} \overline{u} \rangle \left(\boldsymbol{x}', 0\right) = \langle \partial_{x_d} \overline{x_d^p} \rangle \left(\boldsymbol{x}', 0\right) + \langle \partial_{x_d} \overline{U_{\mathrm{B}}} \rangle \left(\boldsymbol{x}', 0\right) = \langle \partial_{x_d} \overline{x_d^p} \rangle \left(\boldsymbol{x}', 0\right))$, we obtain:

$$\langle \partial_{x_d} \overline{u} \rangle \left(\boldsymbol{x}', 0\right) = h^{p-1} \int_{\mathbb{R}_+^d} y_d^{p+1} F\left(|\boldsymbol{y}|\right) d\boldsymbol{y} = h^{p-1} \frac{p C_{p-1}}{2},$$

$$\langle \Delta \overline{u} \rangle_{\mathrm{M}} \left(\boldsymbol{x}', 0\right) = 2 h^{p-2} \int_{\mathbb{R}_+^d} y_d^p F\left(|\boldsymbol{y}|\right) d\boldsymbol{y} = \begin{cases} 2\, M_1\, h^{-1}, & \text{for } p = 1, \\ 1, & \text{for } p = 2, \\ h^{p-2}\left(p-1\right) C_{p-2}, & \text{for } p > 2. \end{cases}$$

$$\langle \Delta \overline{u} \rangle_{\mathrm{MCG}} \left(\boldsymbol{x}', 0\right) = 2\left(d+2\right) h^{p-2} \int_{\mathbb{R}_+^d} \frac{y_d^p y_1^2}{|\boldsymbol{y}|^2} F\left(|\boldsymbol{y}|\right) d\boldsymbol{y}$$

$$= \begin{cases} 2\left(d+2\right) K_1 h^{-1}, & \text{for } p = 1, \\ 1, & \text{for } p = 2, \\ h^{p-2} 2\left(d+2\right) K_p & \text{for } p > 2. \end{cases}$$

3.2. *Antisymmetric extension (ASM)*

Next we consider the antisymmetric extension of u defined as (see Fig. 3):

$$\overline{u}\left(\boldsymbol{x}\right) := \begin{cases} u\left(\boldsymbol{x}\right) & x_d > 0, \\ 2U_{\mathrm{B}} - u\left(\boldsymbol{x}', -x_d\right) & x_d \leq 0. \end{cases}$$

This is the most widespread method to implement the solid BC. In the SPH literature it is generally referred to as the ghost particles (GP) method (e.g. 16), 19), 20)). The expressions for the boundary values are:

$$\langle \overline{u} \rangle \left(\boldsymbol{x}', 0\right) = U_{\mathrm{B}}, \tag{3·11}$$

$$\langle \partial_{x_d} \overline{u} \rangle \left(\boldsymbol{x}', 0\right) = \frac{2}{h} \int_{\mathbb{R}_+^d} u\left(h y_d\right) y_d F\left(|\boldsymbol{y}|\right) d\boldsymbol{y} - \frac{2 U_{\mathrm{B}} M_1}{h}, \tag{3·12}$$

and

$$\langle \Delta \overline{u} \rangle_{\mathrm{M}} \left(\boldsymbol{x}', 0\right) = \langle \Delta \overline{u} \rangle_{\mathrm{MCG}} \left(\boldsymbol{x}', 0\right) = 0. \tag{3·13}$$

We again refer to Appendix B.1 for a justification of these results.

The polynomial profiles $u\left(\boldsymbol{x}\right) = U_{\mathrm{B}} + x_d^p$, $p \geq 1$, behave as:

$$\langle \overline{u} \rangle \left(\boldsymbol{x}', 0\right) = U_{\mathrm{B}},$$
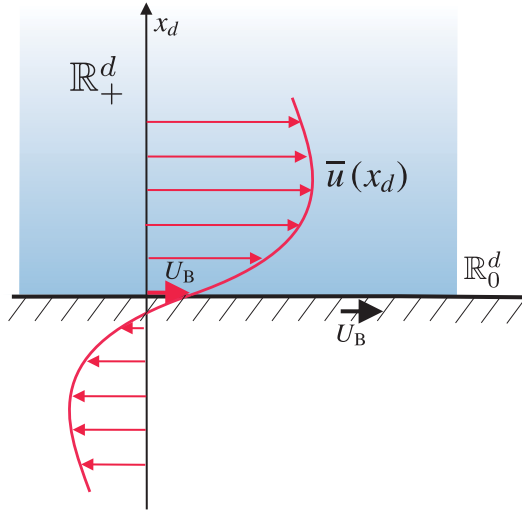
Fig. 3. Antisymmetric extension ASM.

$$\langle \partial_{x_d}\overline{u}\rangle \left(\boldsymbol{x}',0\right) = 2h^{p-1}\int_{\mathbb{R}^d_+} y_d^{p+1}F\left(|\boldsymbol{y}|\right)d\boldsymbol{y}$$

$$= h^{p-1}p\int_{\mathbb{R}^d}|y_d|^{p-1}\,\tilde{W}\left(|\boldsymbol{y}|\right)d\boldsymbol{y} = h^{p-1}pC_{p-1},$$

(the last equality follows from formula (A·7) in Appendix A) and

$$\langle \Delta\overline{u}\rangle_{\mathrm{M}}\left(\boldsymbol{x}',0\right) = \langle \Delta\overline{u}\rangle_{\mathrm{MCG}}\left(\boldsymbol{x}',0\right) = 0.$$

3.3. *Symmetric extension (SSM)*

In this section we deal with the symmetric extension of u defined as (see Fig. 4):

$$\overline{u}\left(\boldsymbol{x}\right) := \begin{cases} u\left(\boldsymbol{x}\right) & x_d > 0, \\ u\left(\boldsymbol{x}', -x_d\right) & x_d \le 0. \end{cases}$$

This procedure is used to enforce a free-slip boundary condition along solid boundaries and, further, is widely applied to mirror the density and pressure fields.[16] Then, for the sake of completeness we include its analysis.

The corresponding formulas for the boundary values are (see Appendix B.1):

$$\langle \overline{u}\rangle \left(\boldsymbol{x}',0\right) = 2\int_{\mathbb{R}^d_+} u\left(hy_d\right)\tilde{W}\left(|\boldsymbol{y}|\right)d\boldsymbol{y}, \tag{3.14}$$

$$\langle \partial_{x_d}\overline{u}\rangle \left(\boldsymbol{x}',0\right) = 0, \tag{3.15}$$

$$\langle \Delta\overline{u}\rangle_{\mathrm{M}}\left(\boldsymbol{x}',0\right) = \frac{2}{h^2}\left[2\int_{\mathbb{R}^d_+} u\left(hy_d\right)F\left(|\boldsymbol{y}|\right)d\boldsymbol{y} - U_{\mathrm{B}}M_0\right], \tag{3.16}$$

$$\langle \Delta\overline{u}\rangle_{\mathrm{MCG}}\left(\boldsymbol{x}',0\right) = \frac{2\left(d+2\right)}{h^2}\left[2\int_{\mathbb{R}^d_+} u\left(hy_d\right)\frac{y_1^2}{|\boldsymbol{y}|^2}F\left(|\boldsymbol{y}|\right)d\boldsymbol{y} - \frac{U_{\mathrm{B}}M_0}{d}\right]. \tag{3.17}$$
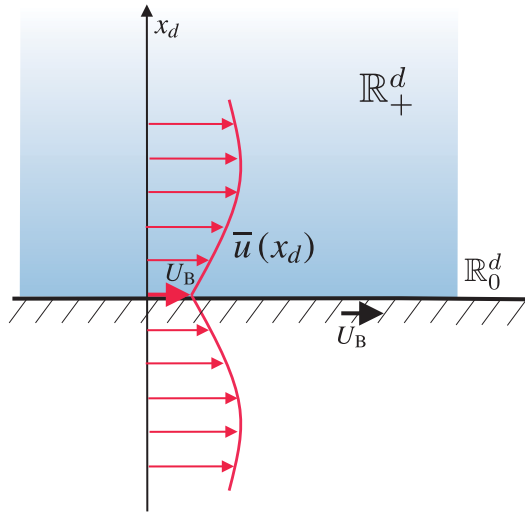
Fig. 4.   Symmetric extension SSM.

If $u\left(\boldsymbol{x}\right) = U_{\mathrm{B}} + x_d^p$ with $p \geq 1$, we obtain, using identities (A·5), (A·6), (A·7) in Appendix A, the following results:

$$\langle \overline{u} \rangle \left(\boldsymbol{x}', 0\right) = U_{\mathrm{B}} + 2h^p \int_{\mathbb{R}_+^d} y_d^p \tilde{W}\left(|\boldsymbol{y}|\right) d\boldsymbol{y} = U_{\mathrm{B}} + h^p C_p,$$

$$\langle \partial_{x_d} \overline{u} \rangle \left(\boldsymbol{x}', 0\right) = 0,$$

$$\langle \Delta \overline{u} \rangle_{\mathrm{M}} \left(\boldsymbol{x}', 0\right) = 4h^{p-2} \int_{\mathbb{R}_+^d} y_d^p F\left(|\boldsymbol{y}|\right) d\boldsymbol{y}$$

$$= \begin{cases} 4\, M_1\, h^{-1}, & \text{for } p = 1, \\ 2, & \text{for } p = 2, \\ h^{p-2} 2\left(p-1\right) C_{p-2}, & \text{for } p > 2. \end{cases}$$

$$\langle \Delta \overline{u} \rangle_{\mathrm{MCG}} \left(\boldsymbol{x}', 0\right) = \begin{cases} 4\left(d+2\right) K_1 h^{-1}, & \text{for } p = 1, \\ 2, & \text{for } p = 2, \\ h^{p-2} 4\left(d+2\right) K_p & \text{for } p > 2. \end{cases}$$

3.4.   *Takeda et al.*[1] *extension*

We define the Takeda et al.[1] extension of a function $u\left(x_d\right)$ by:

$$\overline{u}\left(x_d', x_d\right) := \begin{cases} u\left(x_d'\right) & x_d' > 0, \\ \left(u\left(x_d\right) - U_{\mathrm{B}}\right) \dfrac{x_d'}{x_d} + U_{\mathrm{B}} & x_d' \leq 0, \end{cases}$$

where $x_d > 0$ and $x_d' \in \mathbb{R}$. Note that this extension procedure is slightly different from those previously discussed. Indeed, it associates to each point x_d in the fluid domain an extended field $\overline{u}\left(x_d', x_d\right)$ defined for $x_d' \in \mathbb{R}$ and the extension actually depends on the point x_d. Figure 5 provides an illustration of this procedure.
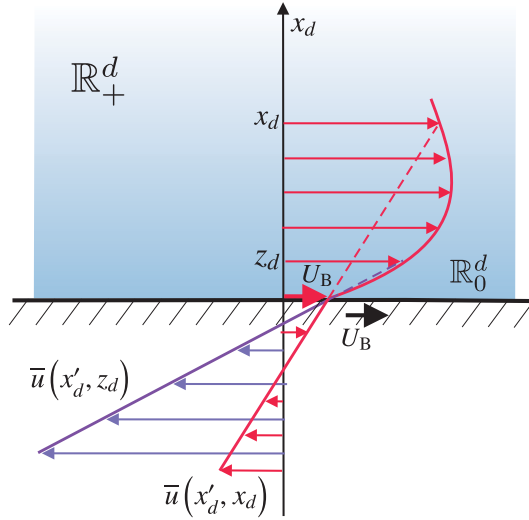
Fig. 5. Takeda et al.[1] extension.

As done before, let $u(x_d) = x_d^p + U_{\mathrm{B}}$ with $p \geq 1$. Clearly, we have:

$$\overline{u}\left(x_d', x_d\right) := \begin{cases} (x_d')^p + U_{\mathrm{B}} & x_d' > 0, \\ x_d^{p-1}x_d' + U_{\mathrm{B}} & x_d' \leq 0. \end{cases}$$

Note that for $p = 1$, we have $\overline{u}(x_d', x_d) = x_d' + U_{\mathrm{B}}$. Now, for $p \geq 2$,

$$\langle \overline{u} \rangle \left(\boldsymbol{x}', 0\right) = U_{\mathrm{B}} + h^p \int_{\mathbb{R}_+^d} y_d^p \tilde{W}\left(|\boldsymbol{y}|\right) d\boldsymbol{y}.$$

The expression for the derivative is the following:

$$\langle \partial_{x_d} \overline{u} \rangle \left(\boldsymbol{x}', 0\right) = h^{p-1} \int_{\mathbb{R}_+^d} y_d^{p+1} F\left(|\boldsymbol{y}|\right) d\boldsymbol{y}.$$

Concerning the Laplacian, we obtain:

$$\langle \Delta \overline{u} \rangle_{\mathrm{M}} \left(\boldsymbol{x}', 0\right) = 2h^{p-2} \int_{\mathbb{R}_+^d} y_d^p F\left(|\boldsymbol{y}|\right) d\boldsymbol{y},$$

and

$$\langle \Delta \overline{u} \rangle_{\mathrm{MCG}} \left(\boldsymbol{x}', 0\right) = 2(d+2) h^{p-2} \int_{\mathbb{R}_+^d} y_d^p \frac{y_1^2}{|\boldsymbol{y}|^2} F\left(|\boldsymbol{y}|\right) d\boldsymbol{y}.$$

Then, using the identity (A·7), we conclude that the boundary values take the following form:

$$\langle \overline{u} \rangle \left(\boldsymbol{x}', 0\right) = \begin{cases} U_{\mathrm{B}} & \text{for } p = 1, \\ U_{\mathrm{B}} + h^p \dfrac{C_p}{2} & \text{for } p > 1, \end{cases}$$

$$\langle \partial_{x_d} \overline{u} \rangle \left(\boldsymbol{x}', 0\right) = \begin{cases} 1 & \text{for } p = 1, \\ h^{p-1} \dfrac{pC_{p-1}}{2} & \text{for } p > 1, \end{cases}$$

Table I. Summary of the results of §3.5.

Mirroring→	U0M				ASM				Takeda et al.[1]			
	p				p				p			
Operator ↓	0	1	2	≥ 3	0	1	2	≥ 3	0	1	2	≥ 3
$\langle u \rangle$	U_B	$U_B + h$	$U_B + h^2$	$U_B + h^p$	U_B	U_B	U_B	U_B	U_B	U_B	$U_B + h^2$	$U_B + h^p$
$\langle \partial_{x_d} u \rangle$	0	1/2	h	h^{p-1}	0	1	h	h^{p-1}	0	1	h	h^{p-1}
$\langle \Delta u \rangle_M$	0	1/h	1	h^{p-2}	0	0	0	0	0	0	1	h^{p-2}
$\langle \Delta u \rangle_{MCG}$	0	1/h	1	h^{p-2}	0	0	0	0	0	0	1	h^{p-2}

Mirroring→	SSM				exact			
	p				p			
Operator ↓	0	1	2	≥ 3	0	1	2	≥ 3
$\langle u \rangle$	U_B	$U_B + h$	$U_B + h^2$	$U_B + h^p$	U_B	U_B	U_B	U_B
$\langle \partial_{x_d} u \rangle$	0	0	0	0	0	1	0	0
$\langle \Delta u \rangle_M$	0	1/h	2	h^{p-2}	0	0	2	0
$\langle \Delta u \rangle_{MCG}$	0	1/h	2	h^{p-2}	0	0	2	0

Table II. Results with the alternative formulation.

Mirroring→	Alternative Takeda				exact			
	p				p			
Operator ↓	0	1	2	≥ 3	0	1	2	≥ 3
$\langle u \rangle$	U_B	U_B	$U_B + h^2$	$U_B + h^p$	U_B	U_B	U_B	U_B
$\langle \partial_{x_d} u \rangle$	0	1	h	h^{p-1}	0	1	0	0
$\langle \Delta u \rangle_M$	0	0	2	h^{p-2}	0	0	2	0
$\langle \Delta u \rangle_{MCG}$	0	0	2	h^{p-2}	0	0	2	0

$$\langle \Delta \overline{u} \rangle_M \left(\boldsymbol{x}', 0 \right) = \begin{cases} 0 & \text{for } p = 1, \\ h^{p-2} \left(p - 1 \right) C_{p-2} & \text{for } p > 1, \end{cases}$$

$$\langle \Delta \overline{u} \rangle_{MCG} \left(\boldsymbol{x}', 0 \right) = \begin{cases} 0 & \text{for } p = 1, \\ h^{p-2} 2 \left(d + 2 \right) K_p & \text{for } p > 1. \end{cases}$$

3.5. Summary of results

A summary of the results obtained in the previous Sections for a velocity field of the type:

$$\boldsymbol{u}(\boldsymbol{x}) := \left(U_B + x_d^p, 0, ..., 0 \right), \quad x_d > 0,$$

as x_d approaches the boundary $x_d = 0$ is presented in Tables I and II. We highlight the following facts:

1. All the mirroring techniques considered in the present work are consistent in the sense that the exact boundary value of the velocity field is recovered as the parameter h tends to zero.

2. When a linear field is mirrored by means of the U0M and SSM models, the boundary values that are obtained for the second derivatives are divergent as h approaches zero. This means that they are inadequate for modeling viscous flows. The reason for this singular behavior is that both the U0M and SSM extensions of a linear field have a discontinuous first derivative. As a consequence, their second derivatives produce delta functions concentrated on $x_d = 0$.

3. The ASM model gives second derivatives that are null at the boundary, regardless of the velocity field considered. This is due to cancellation properties in the integrals defining the SPH approximations and are a consequence of the symmetry of the kernel.
4. The same reasons are responsible for the lack of accuracy on the computation of the first derivatives of a linear field extended by the U0M and SSM techniques.
5. Takeda et al.[1] provides similar results to ASM model with the very significant difference that boundary value of the second derivative of a quadratic field is not null and equals half its exact value.
6. The results obtained using the MCG viscous term do not present any significant difference with those achieved using the M viscous term.
7. Each mirroring technique that produces an extension that is twice differentiable gives satisfactory results for differential operators of order at most two. Anyway, note that this approach is very expensive from the computational point of view.

§4. A novel consistent formulation

In view of the results presented in the previous section, it is clear that none of the considered mirroring techniques allow the first- and second-order SPH operators to converge towards the correct solution when the velocity field has the form (3·1). Anyway, note that the Takeda et al. approximation is consistent up to order one and only fails to give the correct value of the SPH Laplacians on polynomials of order two by a constant factor. A natural way to put remedy to this flaw is to properly renormalize the differential operator. Then let us consider the following functions:

$$L_{M,2}(x_d) = \frac{1}{2} \langle \Delta \overline{v} \rangle_M (\boldsymbol{x}', x_d),$$

$$L_{MCG,2}(x_d) = \frac{1}{2} \langle \Delta \overline{v} \rangle_{MCG} (\boldsymbol{x}', x_d).$$

In the above expressions, $\overline{v}$ stands for the Takeda et al. extension of the quadratic field $v(x_d) := x_d^2 + U_B$. Recall that:

$$\overline{v}(x_d', x_d) = \begin{cases} (x_d')^2 + U_B & x_d' > 0, \\ x_d x_d' + U_B & x_d' \leq 0, \end{cases}$$

and, for instance:

$$L_{M,2}(x_d) = \frac{1}{h^2} \left[\int_{y_d \geq -x_d/h} (x_d + h y_d)^2 F(|\boldsymbol{y}|) \, d\boldsymbol{y} \right.$$

$$\left. + x_d \int_{y_d \leq -x_d/h} (x_d - h y_d) F(|\boldsymbol{y}|) \, d\boldsymbol{y} - x_d^2 \int_{\mathbb{R}^d} F(|\boldsymbol{y}|) \, d\boldsymbol{y} \right] = \frac{1}{2} + R(x_d, h),$$

where the remainder $R(x_d, h) = h^{-1} x_d \int_{y_d \geq -x_d/h} y_d F(|\boldsymbol{y}|) \, d\boldsymbol{y}$ tends to zero faster than any polynomial as $h \to 0^+$.

Note that

$$L_{\text{M},2}(0) = L_{\text{MCG},2}(0) = \frac{1}{2}.$$

We can therefore define the modified Laplacians:

$$\langle \Delta \overline{u} \rangle_{\tilde{\text{M}}} \left(\boldsymbol{x}', x_d \right) = \frac{\langle \Delta \overline{u} \rangle_{\text{M}} \left(\boldsymbol{x}', x_d \right)}{L_{\text{M},2}(x_d)},$$

$$\langle \Delta \overline{u} \rangle_{\tilde{\text{MCG}}} \left(\boldsymbol{x}', x_d \right) = \frac{\langle \Delta \overline{u} \rangle_{\text{MCG}} \left(\boldsymbol{x}', x_d \right)}{L_{\text{MCG},2}(x_d)},$$

which clearly satisfy:

$$\langle \Delta \overline{u} \rangle_{\tilde{\text{M}}} \left(\boldsymbol{x}', 0 \right) = \langle \Delta \overline{u} \rangle_{\tilde{\text{MCG}}} \left(\boldsymbol{x}', 0 \right) = 2,$$

as desired. This result is of great importance since the novel formulation proposed here, being consistent, allows a correct implementation of the no-slip boundary conditions in those problems where the viscous or diffusive terms play a determinant role. Hereinafter the consistent formulation will be named Renormalized Takeda formulation.

§5.   Poiseuille flow

The steady plane Poiseuille flow can be described in $\mathbb{R}^2$ by the mathematical expression (see Batchelor[21]):

$$\triangle u(x_2) = \frac{\nabla P}{\mu}, \tag{5·1}$$

where u is the first component of the unidirectional velocity field $\boldsymbol{u} = (u, 0)$, ∇P is a constant pressure gradient that drives the flow between the two parallel plates towards the increasing x_1 values and μ is the dynamic viscosity. The boundary conditions used for this case will consider $U_B = 0$ for simplicity. The parallel plates will be set at $x_2 = 0$ and $x_2 = 1$ consequently the boundary conditions can be expressed as:

$$u(0) = 0,$$
$$u(1) = 0.$$

The solution to this problem for a pressure gradient, $\frac{\nabla P}{\mu} = -2$, is given by the expression:

$$u(x_2) = x_2(1 - x_2). \tag{5·2}$$

The Poiseuille flow is a sufficient paradigmatic example that presents enough generality and contains the inconsistencies detected in the formulation described before. The solution of a Poiseuille flow is a superposition of a linear velocity field ($p = 1$) plus a quadratic velocity field ($p = 2$).
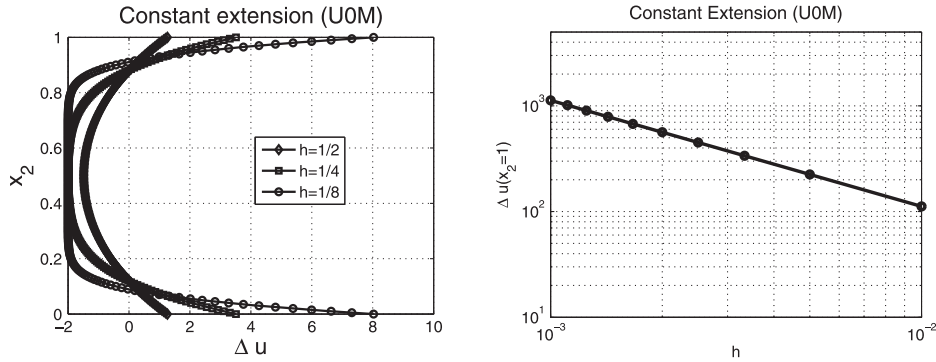
Fig. 6. U0M extension. Left: Laplacian of (5·2). Right: dependence on h of the Laplacian at the boundary.

5.1. *Laplacian of the velocity field for a Poiseuille flow*

Here we check how well the Laplacian of the analytical solution (5·2) is approximated when the mirroring-techniques described in the previous sections are adopted. Similar calculations have been already performed in Souto et al.[15] for the linear Couette flow and for a quadratic field, but in that work the evolution of the kinetic energy was the only variable monitored for the Poiseuille flow. The Laplacian has been evaluated at 200 equidistant points in the interval $[0, 1]$ and the parameter h is varied.

Figure 6 displays the Laplacian of (5·2) when the U0M extension is used. In the left panel, the exact result, that is $\triangle u = -2$, is recovered far from the boundaries while the solution diverges as h decreases. To better inspect the dependence of Laplacian on the parameter h, the right panel show the Laplacian at the boundary (that is, at $x_2 = 1$) using the logarithmic scale. Consistently with the summary shown in Table I, the behavior shows a $1/h$ dependence.

In Fig. 7 all the other possible extensions have also been plotted. The ASM extension reproduces the correct value in the inner domain but it presents an incorrect zero value at the boundary. The SSM extension suffers from the same inconsistency shown by the U0M formulation. The Takeda extension reproduces the correct value in the inner boundary but it fails near the boundary where it goes to -1 instead of -2. Finally, the Renormalized Takeda formulation is able to reproduce the correct value in the whole domain. All these results are in good agreement with those presented in Tables I and II.

5.2. *Numerical simulations of Poiseuille flow*

In this section numerical simulations will be used as a "cross checking" for the theoretical conjectures shown before. A time dependent plane Poiseuille flow can be described in $\mathbb{R}^2$ by the mathematical expression, see:[21]

$$\rho \frac{\partial u(x_2, t)}{\partial t} = -\nabla P + \mu \triangle u(x_2, t), \tag{5·3}$$

where ρ and μ are the fluid density and fluid viscosity respectively.
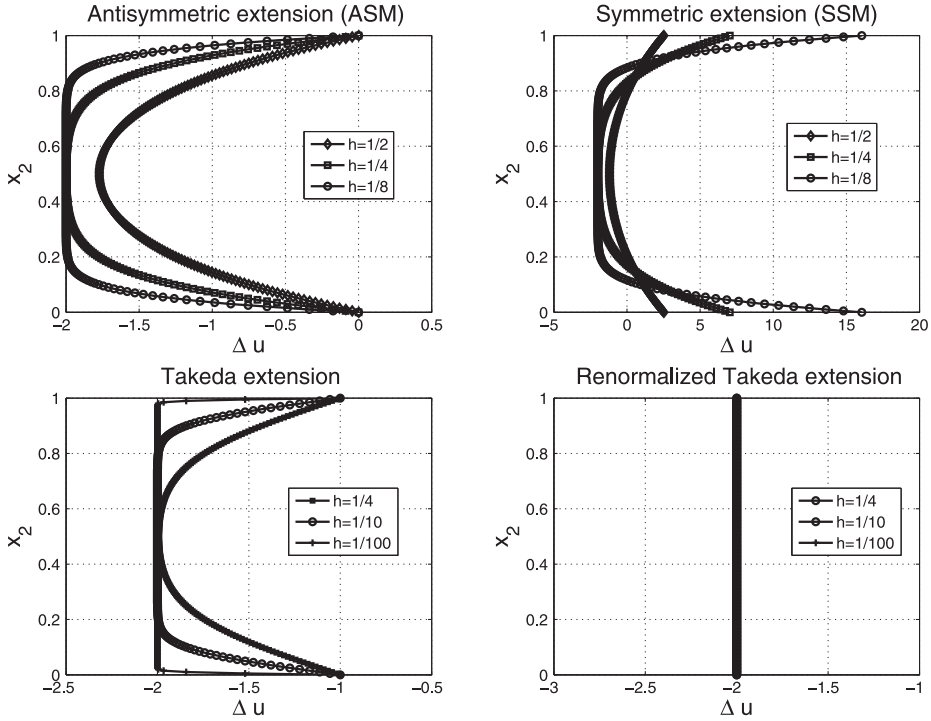
Fig. 7.　Laplacian of (5·2) for the different extensions: ASM, SSM, Takeda et al.[1] and the Renormalized Takeda extension.

Equation (5·3) has been discretized according to the standard SPH formulation in the physical interval $[0,1] \times [0,1]$. Two error sources will be present in the following calculations:[9] first, due to the use of a kernel smoothing function and second, coming from the evaluation of integrals as finite sums. Time integration has been performed using a Leap-frog second order scheme[22] and the selection of the time step has been based on the viscous diffusion and acceleration terms.[22] Periodic conditions have been implemented for the inflow and outflow boundaries. For top and bottom boundaries U0M, ASM and SSM extensions have been imposed after every predictor and corrector loop, while in the Takeda extension the boundary conditions are imposed locally in the viscous force calculation loop. Under the assumption that the flow is horizontal, the discrete SPH form of Eq. (5·3) is (see Basa et al.[20]):

$$\frac{du_a}{dt} = -\nabla P_a + \mathbf{\Pi}_a, \tag{5·4}$$

where the subscript a refers to the particle that carries over the considered property and $\mathbf{\Pi}_a$ represents the viscous interaction. The kernel will be a normalized Gaussian kernel with a support of $3h$:[23]

$$W(r_{ab}, h) = \begin{cases} \dfrac{e^{-\frac{r_{ab}^2}{h^2}}}{\pi h^2} & \text{when} \quad r_{ab} \leq 3h \\ 0 & \text{otherwise,} \end{cases} \tag{5·5}$$

where h is the smoothing length, $\boldsymbol{r_{ab}} = \boldsymbol{r_a} - \boldsymbol{r_b}$ and $r_{ab} = \|\boldsymbol{r_{ab}}\|$ is the Euclidean distance between the two particles. Here, the Morris viscosity model (M)[2] has been used. If the viscosity is constant and a Gaussian kernel is used (see Eq. (5·5)), the term $\boldsymbol{\Pi}_a^M$ has the form:

$$\boldsymbol{\Pi}_a^M = -\sum_{b\in\mathcal{N}_a} m_b \boldsymbol{\Pi}_{ab}^M \nabla_a W_{ab} = -\sum_{b\in\mathcal{N}_a} \frac{4\mu m_b}{\rho_a \rho_b} \frac{W_{ab}}{h^2} \boldsymbol{v_{ab}} \tag{5·6}$$

in which m is the mass, $\boldsymbol{v_{ab}} = \boldsymbol{u_a} - \boldsymbol{u_b}$, b is an a neighbor particle, $\nabla_a W_{ab}$ is the gradient of the b-centered kernel with respect to the coordinates of particle a and $\mathcal{N}_a$ is the set of particle a neighbors.

In each simulation the parameter h is varied while the ratio dx/h is kept constant ($dx/h = 1/40$). The values used for the h parameter are $h = 10/512, 20/512, 40/512$ (U0M and ASM) and $h = 40/512, 80/512, 160/512$ (Takeda and Renormalized Takeda formulation). The stopping criteria used to quit the simulation is:

$$\max_i \{u_i^{k+1} - u_i^k\} \leq 10^{-5}, \tag{5·7}$$

where u_i^k is the velocity value of the fluid particle i at the time step k.

The equation has been simulated in time until the stopping criteria is reached or 12000 time steps are completed. The steady state is reached when the pressure gradient is balanced with the viscous force for all fluid particles. The initial velocity used for the fluid particles is equal to the exact analytical solution $u^0(x_2) = -\frac{\nabla P}{2\mu} x_2(1-x_2)$ in the interval $(0,1)$ and no particle row is set either at $x_2 = 0$ nor at $x_2 = 1$. In the following simulations the values of the pressure gradient and dynamic viscosity were: $\nabla P = -9.8$ and $\mu = 0.744$.

When the U0M extension is used, the viscous force calculated according to the Laplacian operator has a strong $1/h$ dependence near the boundaries (see Table I and Fig. 6). As a consequence, the viscous force felt by the fluid is not computed correctly as h varies. Let us denote by u_b^k and $(\Delta u^k)_b$ the velocity and the Laplacian of the velocity at the k-th time iteration for the particle closest to the boundary respectively. At the zeroth time step, the Laplacian of the exact solution is evaluated at the boundary and, consistently with the results highlighted in Table I, gives a constant expression plus an extra term f that depends on $1/h$ and acts on the boundaries as a driving shear force, see figure 6 for a better comprehension of the $1/h$ dependence.

$$(\Delta u^0)_b = \frac{\nabla P}{2\mu} + f, \tag{5·8}$$

where $f = \frac{-\nabla P}{\mu} \frac{M_1}{h}$.

Assuming $u_b^0 = 0$, this spurious force f creates a local acceleration near the boundaries that increases the local velocity near the boundary as:

$$u_b^1 = u_b^0 + \Delta t \left(-\nabla P + \frac{\nabla P}{2} + \mu f \right) = -\Delta t \nabla P \left(\frac{1}{2} + \frac{M_1}{h} \right) = u_b^{extra,1}. \tag{5·9}$$
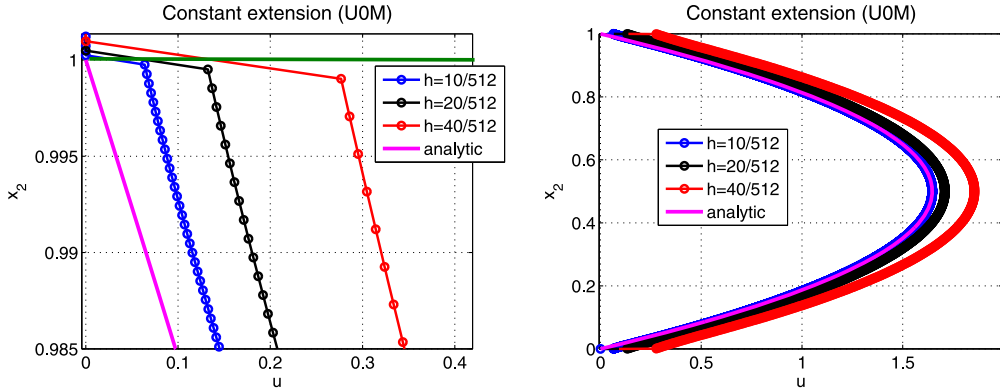
Fig. 8. (color online) U0M extension. Velocity profiles for different values of the parameter h at $x_1 = 0.5$, right: full picture, left: zoomed view in the neighborhood of $x_2 = 1$ (green line).

This extra velocity $u_b^{extra,1}$ is confined near the boundary and prevents the exact analytical solution to verify the discretized equation. At the next time step, a discontinuity at the boundary caused by the extra velocity $u_b^{extra,1}$ and the zero extended field is present. This type of discontinuities are not included in this paper. However, calculations similar to the ones performed in §3 reveal that the Laplacian of such a velocity field gives an extra term at the boundary that is equal to $M_0 u_b^{extra,1}/h^2$. Denoting this term by g, at the first time step we get:

$$(\Delta u^1)_b = O\left(\frac{\nabla P}{2\mu}\right) + O(f) + g. \tag{5.10}$$

Consequently the next time step, the velocity variation at the boundary is:

$$\left(\frac{du}{dt}\right)_b = -\nabla P + O\left(\frac{\nabla P}{2}\right) + \mu\left(O(f) + g\right). \tag{5.11}$$

To obtain the stationary state all forces must be balanced. This requires that the driving forces $-\nabla P + O(\frac{-\nabla P}{2})$ equilibrate the opposite viscous forces $\mu(O(f) + g)$. As a consequence, when the stationary condition is attained, a residual velocity is accumulated near the boundaries. This velocity $u_b^{extra,n}$ has to satisfy:

$$\mu\frac{M_0 u_b^n}{h^2} = O\left(\frac{-\nabla P}{2}\right) + O\left(-\nabla P\frac{M_1}{h}\right). \tag{5.12}$$

This means that when the steady state is reached, a slip velocity $u_b^{extra,n} \sim O(h) + O(h^2)$ remains as an error in the stationary state. Remarkably, the inconsistency due to the U0M extension has been removed thanks to the presence of the extra friction term g and the residual velocity $u_b^{extra,n}$ tends to zero when the smoothing length h decreases.

In Fig. 8 the velocity profiles for three different values of h interpolated at the middle line $x_1 = 0.5$ are shown near the boundary $x_2 = 1$. The h dependence of the velocity profiles can be observed when this kind of extension is used, as h is increased the velocity value is greater at $x_2 = 1$.

Analogously when the SSM extension is used, the viscous force has also a strong $1/h$ dependence near the boundary. This causes that the pressure gradient is not correctly balanced specially near the boundaries where the velocity values over-predict the expected zero value. As before, the result of the first Laplacian applied to the exact solution is a constant expression plus an extra term f that varies as $1/h$ where the boundary is extended and acts as a driving shear force. This force will create an extra velocity $u_b^{extra,1}$. The SSM extension will produce an extended field that will approach $u_b^{extra,1}$ at both sides of the boundary. Consequently, no discontinuity is produced at the boundary and there is no balanced force $g = 0$. As a consequence the velocity grows without convergence and the non-slip boundary condition is lost in the process. Therefore, the SSM extension it is not a suitable approach in order to enforce this boundary condition.

When the ASM extension is used, the viscous force has no dependence on $1/h$, and it is just incorrectly calculated at the boundary where it value goes to zero. The result of the first Laplacian applied to the exact solution is a constant expression that tends to zero where the boundary is extended,

$$(\Delta u^0)_b = 0. \tag{5·13}$$

Due to incorrect calculation of the Laplacian the pressure gradient is not balanced near the boundary by the viscous force. Assuming $u_b^0 = 0$, the lack of friction near the boundary creates a local extra velocity $u^{extra,1}$ as:

$$u_b^1 = u_b^0 - \Delta t \nabla P = u_b^{extra,1}. \tag{5·14}$$

Similarly to the U0M case, $u_b^{extra,1}$ is confined near the boundary and does not allow the exact analytical solution to verify the discretized equation. In the subsequent time step, a discontinuity generates at the boundary between the extra velocity $u_b^{extra,1}$ and the asymmetric extended field. The Laplacian of this extra field g is proportional to $M_0 u_b^{extra,1}/h^2$.

$$(\Delta u^1)_b = (\Delta u^0)_b + (\Delta u^{extra})_b = g. \tag{5·15}$$

Consequently the next time step, the velocity variation at the boundary is:

$$\left(\frac{du}{dt}\right)_b = -\nabla P + \frac{\mu M_0 u_b^{extra,1}}{h^2}. \tag{5·16}$$

To obtain the stationary state the forces $-\nabla P$ and μg must be balanced. As a consequence, the presence of a slip velocity $u_b^{extra,n}$ is necessary to produce a force g that acts in the opposite direction to the driving shear $-\nabla P$, creating a local friction that equilibrates the global momentum. As a result when the stationary condition is obtained a residual velocity is always accumulated near the boundaries. At the equilibrium state, this velocity $u_b^{extra,n}$ should be as

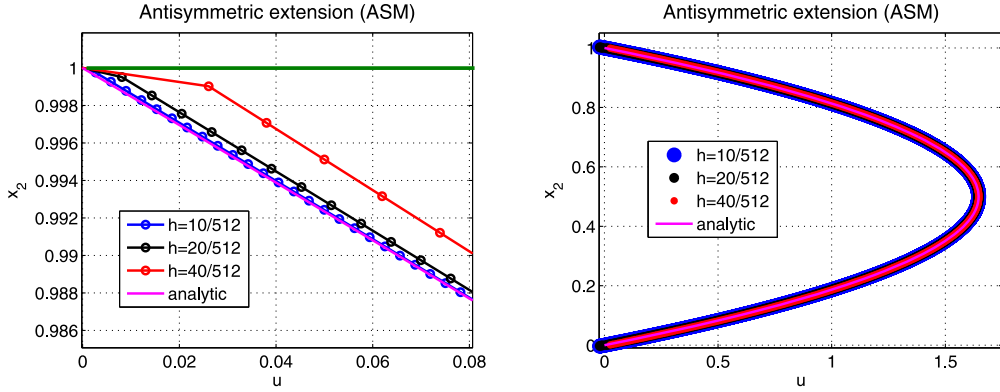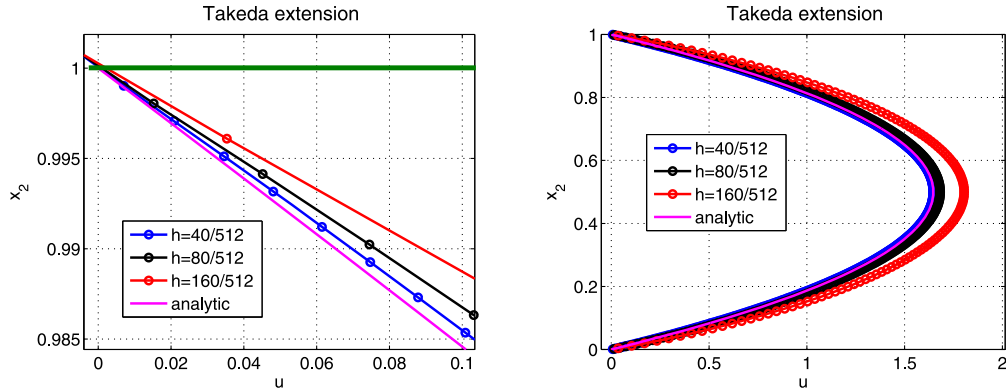$$\frac{\nabla P}{\mu} = \frac{u_b^{extra,n}}{h^2} M_0. \tag{5·17}$$

Fig. 9. (color online) ASM extension. Velocity profiles for different values of the parameter h at $x_1 = 0.5$, right: full picture, left: zoomed view in the neighborhood of $x_2 = 1$ (green line).

This means that $u_b^{extra,n} \sim O(h^2)$ remains as an error in the stationary state.

In Fig. 9 the velocity profiles for three different values of h interpolated at $x_1 = 0.5$ are shown. If we zoom the velocity profiles near the boundary we can observe that they have a h^2 dependence when the ASM extension is used.

When Takeda's extension is used, the result of the first Laplacian applied to the exact solution is a constant expression that tends to one, see Table I,

$$(\triangle u^0)_b = \frac{\nabla P}{2\mu}. \tag{5·18}$$

Assuming $u_b^0 = 0$, the lack of friction near the boundary creates a local extra velocity as:

$$u_b^1 = u_b^0 - \Delta t \nabla P + \Delta t \frac{\nabla P}{2} = u_b^{extra,1}. \tag{5·19}$$

In the subsequent time step, a discontinuity occurs at the boundary between $u_b^{extra,1}$ and the extended field. The Laplacian of this spurious field at the boundary $u_b^{extra,1}$, denoted by g, is proportional to $M_0 u_b^{extra,1}/h^2$

$$(\triangle u^1)_b = (\triangle u^0)_b + (\triangle u^{extra,1})_b = O\left(\frac{\nabla P}{2\mu}\right) + g. \tag{5·20}$$

Consequently the next time step, the variation of the velocity at the boundary is:

$$\left(\frac{du}{dt}\right)_b = -\nabla P + O\left(\frac{\nabla P}{2}\right) + \mu g. \tag{5·21}$$

To obtain the stationary state the forces $-\frac{\nabla P}{2}$ and μg must be balanced. This requires that the force μg is opposite to the driving shear $\frac{\nabla P}{2}$ and creates a local friction that equilibrates the global momentum. As a result when the stationary condition is attained a residual velocity is always accumulated near the boundaries. This velocity $u_b^{extra,n}$ should be as:

$$\frac{\nabla P}{2\mu} = \frac{u_b^{extra,n}}{h^2} M_0. \tag{5·22}$$

Fig. 10. (color online) Takeda extension. Velocity profiles for different values of the parameter h at $x_1 = 0.5$, right: full picture, left: zoomed view in the neighborhood of $x_2 = 1$ (green line). The velocity values out of the fluid domain are not representative due to the local character of the boundary condition.

Similarly to the ASM extension, this means that $u_b^{extra,n} \sim O(h^2)$ and remains as an error in the stationary state.

In Fig. 10 the velocity profiles for three different values of h interpolated at $x_1 = 0.5$ are shown. It must be taken into account that the velocity values out of the fluid domain are not representative due to the local character of the boundary condition.

Finally, if the Renormalized Takeda formulation is used, the result of the first Laplacian applied to the exact solution is $\frac{\nabla P}{\mu}$ everywhere.

$$(\triangle u^0)_b = \frac{\nabla P}{\mu}, \tag{5·23}$$

which balances exactly the pressure gradient in all the fluid domain. The differential equation is well solved and the boundary condition matches for all h values, see Fig. 11.

This example permits to show that most of the extensions (U0M, ASM and Takeda) present an h or an h^2 dependence when they are implemented. Consequently, it seems that the damage is restricted to areas of size h in the vicinity of the boundaries. A problem of order h is not always a small problem in SPH, due to the fact that in many situations a distance h contains a number of particles $\sim h/dx$ where wrong fluid mechanics is performed. The Renormalized Takeda formulation eliminates the h dependence and the velocity profiles match the expected boundary conditions.

§6. Flow past a circular cylinder

Here we analyze the evolution of the flow past a circular cylinder and compare the results obtained by using the various formulations and mirroring techniques studied in the previous sections. In all the cases, $Re = UD/\nu = 200$ (D is the
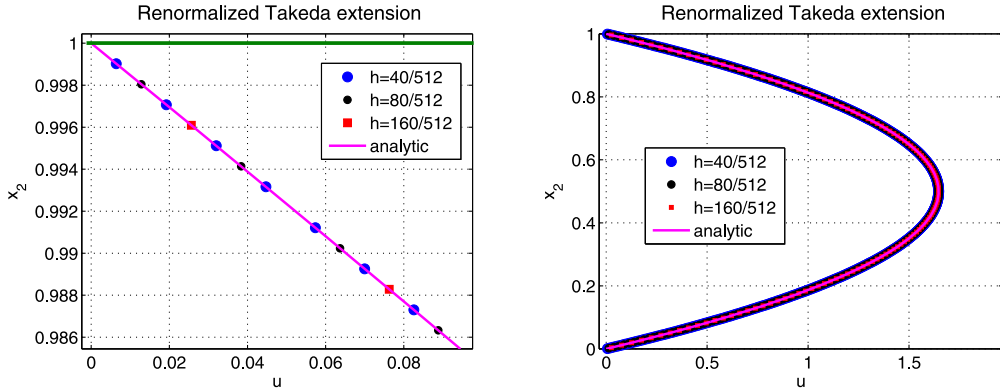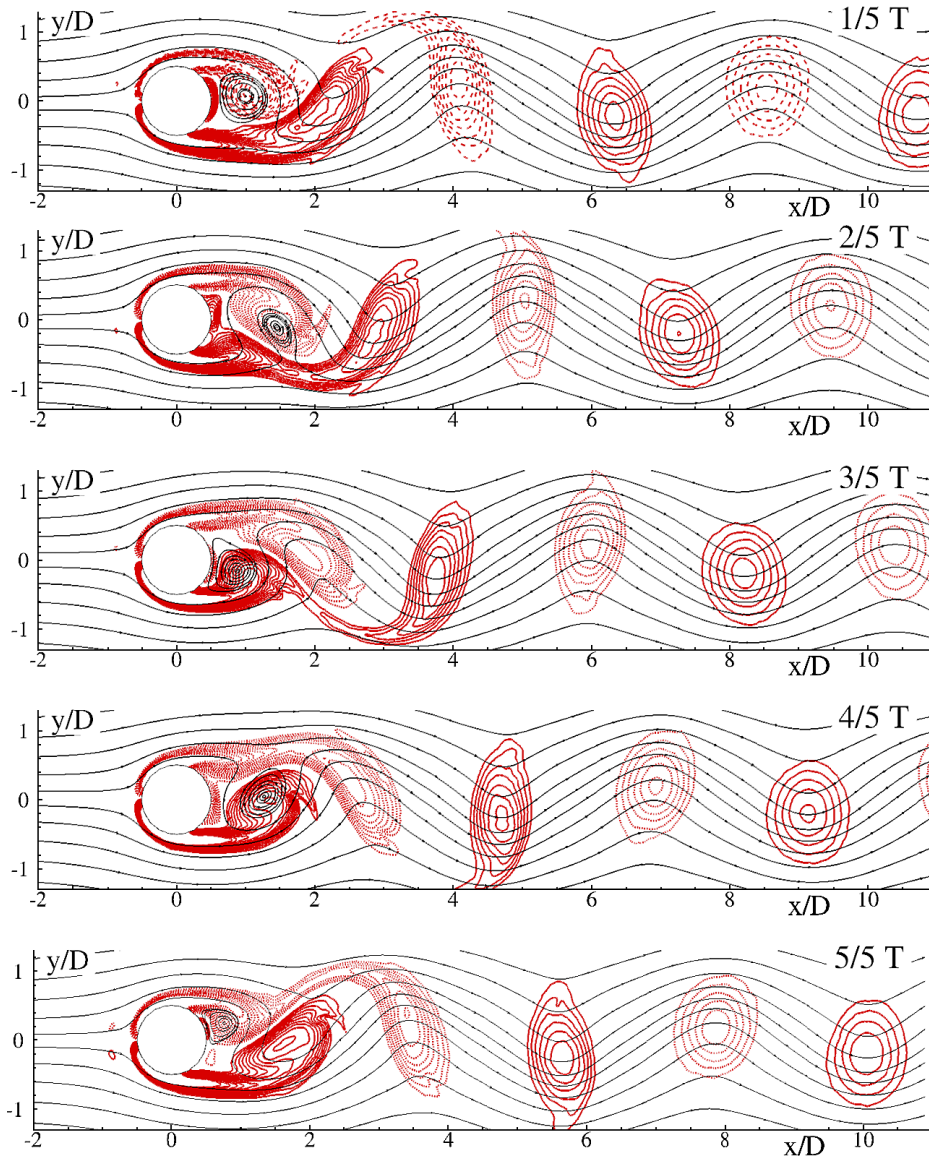
Fig. 12. Stream lines and vorticity contours around a circular cylinder for $Re = 200$ (D is the cylinder diameter and T is the vortex shedding period). The Laplacian of the velocity field has been modeled using the Renormalized Takeda formulation.

coefficients (C_D and C_L respectively) and the Strouhal number St predicted by numerical simulations and experimental measurements available in the literature for $Re = 200$. These are compared with the results obtained by using the Renormalized Takeda formulation for three different spatial resolutions. This analysis shows that the novel formulation rapidly reaches converged values for C_D, C_L and St and, further, that these values are in good agreement with those available in the literature.

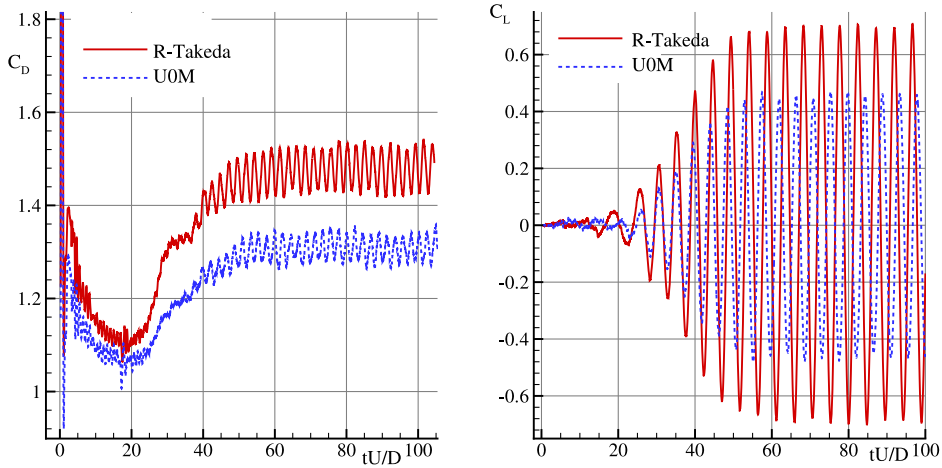With respect to the Renormalized Takeda formulation both the U0M and ASM

Fig. 13.   Drag (left) and Lift (left) coefficients as predicted by using the Renormalized Takeda formulation (solid lines) and the U0M mirroring technique (dashed lines). Here, $D/dx = 80$.
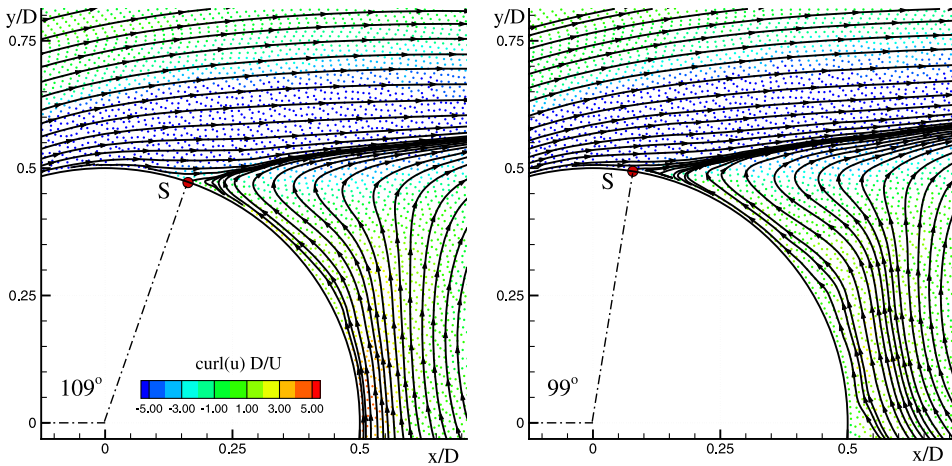

Fig. 14.   Minimum separation angle as predicted by using the Renormalized Takeda formulation (left panel) and the ASM mirroring technique (right panel). Here, $D/dx = 80$.

techniques show some inaccuracies. Specifically, the U0M technique underestimates both the drag and lift coefficients (see Fig. 13) and, therefore, seems to be less accurate in the prediction of the global loads and global quantities in general. Conversely, the ASM technique shows some inaccuracy in the description of the local features of the flow. For example, it tends to underestimate the minimum separation angle (see Fig. 14). Wu et al.[36] predicted this angle to be around 107 degrees (both experiments and numerical simulations were performed) while the simulations with the ASM technique shows an angle of about 99 degrees. In this case, the angle predicted through the Renormalized Takeda formulation is around 109 degrees and, therefore, is in good agreement with the results of Wu et al.[36]

§7.   Conclusions and future work

A rigorous mathematical description of the effect of extending unidirectional velocity fields by mirroring techniques to impose no slip boundary conditions in SPH has been presented. The analytical extension has been performed by using the most representative mirroring techniques, namely dummy particles, ghost particles with symmetric and antisymmetric velocity mirroring and the Takeda et al.[1] boundary integrals. The behavior of the most common operators (function approximation, gradient and Laplacian) of the SPH continuous approximation of the fluid mechanics equations have been analyzed using a general differentiable flow field. On the basis of the fact that the exact representation of the SPH operators should be recovered when the smoothing length parameter h tends to zero, the dependence of these results on h has been studied. According to the calculations performed, the following conclusions can be drawn:

1. The SPH approximation of the velocity fields is consistent in all the extensions.
2. Inconsistencies in the SPH integral representation of the differential operators (gradient and Laplacian) have been found for linear and quadratic fields near the solid boundary. Such inconsistencies are caused by the extension of the velocity field to the whole domain which creates a point at the boundary where the first and/or second derivative are not well defined. For some combinations of flow fields and mirroring techniques, they can appear either as incorrect values on the evaluation of those operators (average value between discontinuous derivative at both sides) or as singularities (presence of Dirac delta functions at the boundary). These results do not depend on the viscosity model used. As a consequence, this means that in some cases there is no convergence towards the exact equations as the resolution and the number of neighbors are simultaneously increased in the numerical computations (e.g. Colagrossi et al.[14] and Souto et al.[15])
3. The Renormalized Takeda extension permits a consistent redefinition such that all the operators converge towards the correct values. This original result shows that in those problems where the Laplacian operator plays an important physical role, a consistent implementation of the no-slip boundary conditions is possible.

The theoretical inconsistencies summarized above are the main cause of the inaccuracies observed in the numerical test cases of §§5 and 6. This further proves the relevance of the present study for practical applications of SPH schemes.

Acknowledgements

Appendix A
—— *Integral Identities* ——

1. By symmetry, since F is a radial function,

$$\int_{\mathbb{R}^d} \varphi\left(\boldsymbol{y}\right) F\left(|\boldsymbol{y}|\right) d\boldsymbol{y} = 0, \tag{A·1}$$

for any function φ such that $\varphi\left(y_1, .., -y_k, ..., y_d\right) = -\varphi\left(\boldsymbol{y}\right)$.

2. Another useful identity is the one concerning the second moments of $F\left(|\boldsymbol{x}|\right)$. By definition,

$$x_k F\left(|\boldsymbol{x}|\right) = -\partial_{x_k} \tilde{W}\left(|\boldsymbol{x}|\right), \tag{A·2}$$

and integration by parts gives:

$$\int_{\mathbb{R}^d} x_k^2 F\left(|\boldsymbol{x}|\right) d\boldsymbol{x} = -\int_{\mathbb{R}^d} x_k \partial_{x_k} \tilde{W}\left(|\boldsymbol{x}|\right) d\boldsymbol{x} = 1, \tag{A·3}$$

therefore, summing over k we get:

$$\int_{\mathbb{R}^d} |\boldsymbol{x}|^2 F\left(|\boldsymbol{x}|\right) d\boldsymbol{x} = d. \tag{A·4}$$

3. Now, we compute the moments of $F\left(|\boldsymbol{x}|\right)$ on the half-space $\mathbb{R}^d_+$. After using (A·2) and integrating by parts, we find that the first moment is given by:

$$\int_{\mathbb{R}^d_+} x_d F\left(|\boldsymbol{x}|\right) d\boldsymbol{x} = \int_{\mathbb{R}^d_0} \tilde{W}\left(|\boldsymbol{x}'|\right) d\boldsymbol{x}'. \tag{A·5}$$

In view of (A·3) and the radiality of the integrand, the second moment equals:

$$\int_{\mathbb{R}^d_+} x_d^2 F\left(|\boldsymbol{x}|\right) d\boldsymbol{x} = \frac{1}{2}. \tag{A·6}$$

Finally, combining (A·2) and integration by parts, we have for $p > 2$:

$$\int_{\mathbb{R}^d_+} x_d^p F\left(|\boldsymbol{x}|\right) d\boldsymbol{x} = -\int_{\mathbb{R}^d_+} x_d^{p-1} \partial_{x_d} \tilde{W}\left(|\boldsymbol{x}|\right) d\boldsymbol{x}$$

$$= (p-1) \int_{\mathbb{R}^d_+} x_d^{p-2} \tilde{W}\left(|\boldsymbol{x}|\right) d\boldsymbol{x} = \frac{(p-1)}{2} \int_{\mathbb{R}^d} |x_d|^{p-2} \tilde{W}\left(|\boldsymbol{x}|\right) d\boldsymbol{x}. \tag{A·7}$$

4. The following integrals appear when dealing with the Monaghan-Cleary-Gingold[3)] approximation of the Laplacian.

$$\int_{\mathbb{R}^d} \frac{x_1^2 x_d^2}{|\boldsymbol{x}|^2} F\left(|\boldsymbol{x}|\right) d\,\boldsymbol{x} = \frac{1}{d+2},$$

$$\int_{\mathbb{R}^d_+} \frac{x_1^2 x_d^2}{|\boldsymbol{x}|^2} F\left(|\boldsymbol{x}|\right) d\,\boldsymbol{x} = \frac{1}{2\left(d+2\right)}, \tag{A·8}$$

$$\int_{\mathbb{R}^d} \frac{x_1^2}{|\boldsymbol{x}|^2} F\left(|\boldsymbol{x}|\right) d\boldsymbol{x} = \frac{1}{d} \int_{\mathbb{R}^d} F\left(|\boldsymbol{x}|\right) d\boldsymbol{x},$$

$$\int_{\mathbb{R}^d_+} \frac{x_1^2}{|\boldsymbol{x}|^2} F\left(|\boldsymbol{x}|\right) d\boldsymbol{x} = \frac{1}{2d} \int_{\mathbb{R}^d} F\left(|\boldsymbol{x}|\right) d\boldsymbol{x}. \tag{A·9}$$

For the sake of completeness, we prove the identity (A·8). Note that, using the generalized spherical coordinates and using (A·4), we get:

$$\int_{\mathbb{R}^d} \frac{x_1^2 x_d^2}{|\boldsymbol{x}|^2} F\left(|\boldsymbol{x}|\right) d\boldsymbol{x} = \int_{\mathbb{S}^{d-1}} \theta_1^2 \theta_d^2 d\theta \int_0^\infty r^{d+1} F\left(r\right) dr = \frac{d}{\omega_d} \int_{\mathbb{S}^{d-1}} \theta_1^2 \theta_d^2 d\theta, \tag{A·10}$$

where ω_d denotes the volume of the $(d-1)$-dimensional sphere. Therefore, it suffices to compute the spherical integral on the right hand side of (A·10). By symmetry, we have that:

$$\omega_d = \int_{\mathbb{S}^{d-1}} \left(\sum_{j=1}^d \theta_j^2\right)^2 d\theta = d\left(d-1\right) \int_{\mathbb{S}^{d-1}} \theta_1^2 \theta_d^2 d\theta + d \int_{\mathbb{S}^{d-1}} \theta_1^4 d\theta; \tag{A·11}$$

and, applying a rotation of angle $\pi/4$ on the plane containing the directions θ_1 and θ_d, we get:

$$\int_{\mathbb{S}^{d-1}} \theta_1^2 \theta_d^2 d\theta = \int_{\mathbb{S}^{d-1}} \left[\left(\theta_1^2 - \theta_d^2\right) \frac{1}{2} \sin \frac{\pi}{2} + \theta_1 \theta_d \cos \frac{\pi}{2}\right]^2 d\theta = \frac{1}{4} \int_{\mathbb{S}^{d-1}} \left(\theta_1^2 - \theta_d^2\right)^2 d\theta. \tag{A·12}$$

Collecting terms of the identity above, we conclude that:

$$\int_{\mathbb{S}^{d-1}} \theta_1^2 \theta_2^2 d\theta = \frac{1}{3} \int_{\mathbb{S}^{d-1}} \theta_1^4 d\theta. \tag{A·13}$$

This, together with identity (A·11), gives:

$$\int_{\mathbb{S}^{d-1}} \theta_1^2 \theta_2^2 d\theta = \frac{\omega_d}{d\left(d+2\right)}, \tag{A·14}$$

and the result follows immediately.

Appendix B
—— *Alternative Equivalent Representation of Continuous SPH Operators* ——

In this appendix we gather some equivalent formulations of the continuous SPH approximations of differential operators that are useful in deriving the main results of this article.

- *First-order derivatives.* After a change of variables, expression (2·8) may be rewritten as:

$$\langle \partial_{x_k} u \rangle \left(\boldsymbol{x}\right) = \frac{1}{h^{d+1}} \int_{\mathbb{R}^d} u\left(\boldsymbol{x}'\right) \frac{x_k' - x_k}{h} F\left(\frac{|\boldsymbol{x}' - \boldsymbol{x}|}{h}\right) d\boldsymbol{x}' \tag{B·1a}$$

$$= \frac{1}{h} \int_{\mathbb{R}^d} u\left(\boldsymbol{x} + h\boldsymbol{y}\right) y_k F\left(|\boldsymbol{y}|\right) d\boldsymbol{y}. \tag{B·1b}$$

- *The Laplacian.* Analogously, the expression (2·10) for the Laplacian can be simplified as follows:

$$\langle \Delta u \rangle_{\mathrm{M}}\left(\boldsymbol{x}\right) = \frac{2}{h^{d+2}} \int_{\mathbb{R}^d} \left(u\left(\boldsymbol{x}'\right) - u\left(\boldsymbol{x}\right)\right) F\left(\frac{|\boldsymbol{x}' - \boldsymbol{x}|}{h}\right) d\boldsymbol{x}', \tag{B·2a}$$

$$= \frac{2}{h^2} \int_{\mathbb{R}^d} \left(u\left(\boldsymbol{x} + h\boldsymbol{y}\right) - u\left(\boldsymbol{x}\right)\right) F\left(|\boldsymbol{y}|\right) d\boldsymbol{y}. \tag{B·2b}$$

- *The Monaghan-Cleary-Gingold[3] Laplacian.* The jth component of the Laplacian (2·12) of the velocity field $\boldsymbol{u}$ can be written as:

$$\langle \Delta \boldsymbol{u} \rangle_{\mathrm{MCG}}^j \left(\boldsymbol{x}\right)$$
$$= \frac{2(d+2)}{h^{d+2}} \int_{\mathbb{R}^d} \frac{(\boldsymbol{x}' - \boldsymbol{x}) \cdot (\boldsymbol{u}\left(\boldsymbol{x}'\right) - \boldsymbol{u}\left(\boldsymbol{x}\right))}{|\boldsymbol{x}' - \boldsymbol{x}|^2} F\left(\frac{|\boldsymbol{x}' - \boldsymbol{x}|}{h}\right) \left(x_j' - x_j\right) d\boldsymbol{x}' \tag{B·3a}$$
$$= \frac{2(d+2)}{h^2} \int_{\mathbb{R}^d} \frac{\boldsymbol{y} \cdot (\boldsymbol{u}\left(\boldsymbol{x} + h\boldsymbol{y}\right) - \boldsymbol{u}\left(\boldsymbol{x}\right))}{|\boldsymbol{y}|^2} F\left(|\boldsymbol{y}|\right) y_j d\boldsymbol{y}. \tag{B·3b}$$

Consequently, it follows that:

$$\langle \Delta \boldsymbol{u} \rangle_{\mathrm{MCG}}^1 \left(\boldsymbol{x}\right) = \frac{2\left(d+2\right)}{h^2} \int_{\mathbb{R}^d} \left(u\left(x_d + hy_d\right) - u\left(x_d\right)\right) \frac{y_1^2}{|\boldsymbol{y}|^2} F\left(|\boldsymbol{y}|\right) d\boldsymbol{y}, \tag{B·4}$$

and

$$\langle \Delta \boldsymbol{u} \rangle_{\mathrm{MCG}}^j = 0, \quad \text{for } j = 2, ..., d. \tag{B·5}$$

Let us compare the formulas for the SPH Laplacian (B·2b) and (B·4) with the well-known exact formula based on the mean:

$$\Delta u\left(\boldsymbol{x}\right) = \frac{2d}{h^2} \left[\frac{d}{\omega_d} \int_{|\boldsymbol{y}| \leq 1} u\left(\boldsymbol{x} + h\boldsymbol{y}\right) d\boldsymbol{y} - u\left(\boldsymbol{x}\right) \right] + \mathcal{O}\left(h^2\right), \tag{B·6}$$

where, recall, ω_d stands for the volume of the unit sphere in $\mathbb{R}^d$. Note that this formula can be obtained by replacing the function $F\left(|\boldsymbol{x}|\right)$ with the characteristic function of the unit ball in $\mathbb{R}^d$.

B.1. *Derivation of the main results*

In the following, we deduce the various expressions presented in §2.

1. *Constant extension.* The expression for the derivative is the following:

$$\langle \partial_{x_k} \overline{u} \rangle \left(\boldsymbol{x}', 0\right) = \frac{1}{h} \int_{\mathbb{R}_+^d} u\left(hy_d\right) y_k F\left(|\boldsymbol{y}|\right) d\boldsymbol{y} - \frac{U_{\mathrm{B}}}{h} \int_{\mathbb{R}_+^d} y_k F\left(|\boldsymbol{y}|\right) d\boldsymbol{y}. \tag{B·7}$$

Consequently, the expression (3·8) is obtained from the identity (A·5). Regarding the approximations of the Laplacian, we get:

$$\langle \Delta \overline{u} \rangle_{\mathrm{M}} \left(\boldsymbol{x}', 0\right)$$

$$= \frac{2}{h^2} \left[\int_{\mathbb{R}^d_+} u\,(hy_d)\,F\,(|\boldsymbol{y}|)\,d\boldsymbol{y} + U_{\mathrm{B}} \int_{\mathbb{R}^d_+} F\,(|\boldsymbol{y}|)\,d\boldsymbol{y} - u\,(0) \int_{\mathbb{R}^d} F\,(|\boldsymbol{y}|)\,d\boldsymbol{y} \right]$$

$$= \frac{2}{h^2} \left[\int_{\mathbb{R}^d_+} u\,(hy_d)\,F\,(|\boldsymbol{y}|)\,d\,\boldsymbol{y} - U_{\mathrm{B}} \int_{\mathbb{R}^d_+} F\,(|\boldsymbol{y}|)\,d\boldsymbol{y} \right]$$

$$= \frac{2}{h^2} \left[\int_{\mathbb{R}^d_+} u\,(hy_d)\,F\,(|\boldsymbol{y}|)\,d\,\boldsymbol{y} - \frac{U_{\mathrm{B}}}{2} \int_{\mathbb{R}^d} F\,(|\boldsymbol{y}|)\,d\boldsymbol{y} \right],$$

$$\langle \Delta \overline{u} \rangle_{\mathrm{MCG}}\,(\boldsymbol{x}', 0)$$

$$= \frac{2\,(d+2)}{h^2} \left[\int_{\mathbb{R}^d_+} u\,(hy_d)\,\frac{y_1^2}{|\boldsymbol{y}|^2} F\,(|\boldsymbol{y}|)\,d\boldsymbol{y} + U_{\mathrm{B}} \int_{\mathbb{R}^d_+} \frac{y_1^2}{|\boldsymbol{y}|^2} F\,(|\boldsymbol{y}|)\,d\boldsymbol{y} \right.$$

$$\left. - u\,(0) \int_{\mathbb{R}^d} \frac{y_1^2}{|\boldsymbol{y}|^2} F\,(|\boldsymbol{y}|)\,d\boldsymbol{y} \right]$$

$$= \frac{2\,(d+2)}{h^2} \left[\int_{\mathbb{R}^d_+} u\,(hy_d)\,\frac{y_1^2}{|\boldsymbol{y}|^2} F\,(|\boldsymbol{y}|)\,d\boldsymbol{y} - U_{\mathrm{B}} \int_{\mathbb{R}^d_+} \frac{y_1^2}{|\boldsymbol{y}|^2} F\,(|\boldsymbol{y}|)\,d\boldsymbol{y} \right]$$

$$= \frac{2\,(d+2)}{h^2} \left[\int_{\mathbb{R}^d_+} u\,(hy_d)\,\frac{y_1^2}{|\boldsymbol{y}|^2} F\,(|\boldsymbol{y}|)\,d\boldsymbol{y} - \frac{U_{\mathrm{B}}}{2d} \int_{\mathbb{R}^d} F\,(|\boldsymbol{x}|)\,d\boldsymbol{x} \right], \tag{B·8}$$

the last identity being a consequence of Eq. (A·9).

2. *Antisymmetric extension.* We now derive the expressions for the boundary values for the ASM mirroring.

$$\langle \overline{u} \rangle\,(\boldsymbol{x}', 0) = \int_{\mathbb{R}^d_+} u\,(hy_d)\,\tilde{W}\,(|\boldsymbol{y}|)\,d\boldsymbol{y} + \int_{\mathbb{R}^d_+} [2U_{\mathrm{B}} - u\,(hy_d)]\,\tilde{W}\,(|\boldsymbol{y}|)\,d\boldsymbol{y}$$

$$= 2U_{\mathrm{B}} \int_{\mathbb{R}^d_+} \tilde{W}\,(|\boldsymbol{y}|)\,d\boldsymbol{y} = U_{\mathrm{B}}.$$

The derivative is given by

$$\langle \partial_{x_d} \overline{u} \rangle\,(\boldsymbol{x}', 0) = \frac{1}{h} \int_{\mathbb{R}^d_+} u\,(hy_d)\,y_d F\,(|\boldsymbol{y}|)\,d\boldsymbol{y} - \frac{1}{h} \int_{\mathbb{R}^d_+} (2U_{\mathrm{B}} - u\,(hy_d))\,y_d F\,(|\boldsymbol{y}|)\,d\boldsymbol{y}$$

$$= \frac{2}{h} \int_{\mathbb{R}^d_+} u\,(hy_d)\,y_d F\,(|\boldsymbol{y}|)\,d\boldsymbol{y} - \frac{2U_{\mathrm{B}}}{h} \int_{\mathbb{R}^d_+} y_d F\,(|\boldsymbol{y}|)\,d\boldsymbol{y}, \tag{B·9}$$

where the identity (A·5) has been used to get the last equality. The approximations of the Laplacian behave as:

$$\langle \Delta \overline{u} \rangle_{\mathrm{M}}\,(\boldsymbol{x}', 0) = \frac{2}{h^2} \left(\int_{\mathbb{R}^d_+} u\,(hy_d)\,F\,(|\boldsymbol{y}|)\,d\boldsymbol{y} - \int_{\mathbb{R}^d_+} u\,(hy_d)\,F\,(|\boldsymbol{y}|)\,d\boldsymbol{y} \right.$$

$$\left. + 2U_{\mathrm{B}} \int_{\mathbb{R}^d_+} F\,(|\boldsymbol{y}|)\,d\boldsymbol{y} - U_{\mathrm{B}} \int_{\mathbb{R}^d} F(|\boldsymbol{y}|)d\boldsymbol{y} \right) = 0.$$

An analogous reasoning gives $\langle\Delta\overline{u}\rangle_{\mathrm{MC}}(\boldsymbol{x}',0) = 0$ for the Monaghan-Cleary-Gingold[3] approximation.

3. *Symmetric extension.* The formulas for the SSM mirroring are derived in the following. Since $\overline{u}$ is even in x_d, we get

$$\langle\overline{u}\rangle\left(\boldsymbol{x}',0\right) = 2\int_{\mathbb{R}^d_+} u\left(hy_d\right)\tilde{W}\left(|\boldsymbol{y}|\right)d\boldsymbol{y}.$$

Now,

$$\langle\partial_{x_d}\overline{u}\rangle\left(\boldsymbol{x}',0\right) = \frac{1}{h}\int_{\mathbb{R}^d_+} u\left(hy_d\right)y_dF\left(|\boldsymbol{y}|\right)d\boldsymbol{y} - \frac{1}{h}\int_{\mathbb{R}^d_+} u\left(hy_d\right)y_dF\left(|\boldsymbol{y}|\right)d\boldsymbol{y} = 0.$$

The Laplacian behaves as:

$$\langle\Delta\overline{u}\rangle_{\mathrm{M}}\left(\boldsymbol{x}',0\right)$$
$$= \frac{2}{h^2}\left(\int_{\mathbb{R}^d_+} u\left(hy_d\right)F\left(|\boldsymbol{y}|\right)d\boldsymbol{y} + \int_{\mathbb{R}^d_+} u\left(hy_d\right)F\left(|\boldsymbol{y}|\right)d\boldsymbol{y} - U_{\mathrm{B}}\int_{\mathbb{R}^d} F\left(|\boldsymbol{y}|\right)d\boldsymbol{y}\right)$$
$$= \frac{2}{h^2}\left[2\int_{\mathbb{R}^d_+} u\left(hy_d\right)F\left(|\boldsymbol{y}|\right)d\boldsymbol{y} - U_{\mathrm{B}}\int_{\mathbb{R}^d} F\left(|\boldsymbol{y}|\right)d\boldsymbol{y}\right].$$

For what concerns the Monaghan-Cleary-Gingold approximation of the Laplacian, using identity (A·9) we get:

$$\langle\Delta\overline{u}\rangle_{\mathrm{MCG}}\left(\boldsymbol{x}',0\right)$$
$$= \frac{2\left(d+2\right)}{h^2}\left[2\int_{\mathbb{R}^d_+} u\left(hy_d\right)\frac{y_1^2}{|\boldsymbol{y}|^2}F\left(|\boldsymbol{y}|\right)d\boldsymbol{y} - U_{\mathrm{B}}\int_{\mathbb{R}^d}\frac{y_1^2}{|\boldsymbol{y}|^2}F\left(|\boldsymbol{y}|\right)d\boldsymbol{y}\right]$$
$$= \frac{2\left(d+2\right)}{h^2}\left[2\int_{\mathbb{R}^d_+} u\left(hy_d\right)\frac{y_1^2}{|\boldsymbol{y}|^2}F\left(|\boldsymbol{y}|\right)d\boldsymbol{y} - \frac{U_{\mathrm{B}}}{d}\int_{\mathbb{R}^d} F\left(|\boldsymbol{y}|\right)d\boldsymbol{y}\right].$$

References

1) H. Takeda, S. M. Miyama and M. Sekiya, Prog. Theor. Phys. **92** (1994), 939.
2) J. P. Morris, P. J. Fox and Y. Zhu, J. Comput. Phys. **136** (1997), 214.
3) J. J. Monaghan and D. J. Price, Mon. Not. R. Astron. Soc. **365** (2005), 199, http://dx.doi.org/10.1111/j.1365-2966.2005.09783.x
4) J. J. Monaghan, Rep. Prog. Phys. **68** (2005), 1703.
5) J. Bonet and M. Rodriguez-Paz, J. Comput. Phys. **209** (2005), 541.
6) T. Belytschko, Y. Krongauz, D. Organ, M. Fleming and P. Krysl, Comput. Methods Appl. Mech. Engrg. **139** (1996), 3.
7) C. S. Peskin, J. Comput. Phys. **10** (1972), 252, http://dx.doi.org/10.1016/0021-9991(72)90065-4
8) A. Colagrossi, M. Antuono and D. L. Touzé, Phys. Rev. E **79** (2009), 056701.
9) N. J. Quinlan, M. Basa and M. Lastiwka, International J. Numerical Methods in Engineering **66** (2006), 2064, http://dx.doi.org/10.1002/nme.1617
10) G. Dilts, International J. Numerical Methods in Engineering **44** (1999), 1115.
11) G. A. Dilts, International J. Numerical Methods in Engineering **48** (2000), 1503.

12) F. Macià, J. M. Sánchez, A. Souto-Iglesias and L. M. González, International J. Numerical Methods in Fluids, submitted.

13) A. Amicarelli, F. Leboeuf, L. Fang, J. Caro, J. C. Marongiu and J. Leduc, *5th ERCOFTAC SPHERIC workshop on SPH applications, 2010*, p. 178.

14) A. Colagrossi, L. Delorme, G. Colicchio, A. Souto-Iglesias and J. L. Cercós-Pita, 3rd *ERCOFTAC SPHERIC workshop on SPH applications, June 4-6, 2008*, p. 221.

15) A. Souto-Iglesias, L. M. González, A. Colagrossi and M. Antuono, *5th ERCOFTAC SPHERIC workshop on SPH applications, 2010*.

16) A. Colagrossi and M. Landrini, J. Comput. Phys. **191** (2003), 448.

17) X. Y. Hu and N. A. Adams, Phys. Fluids **18** (2006), 101702.

18) P. Español and M. Revenga, Phys. Rev. E **67** (2003), 026705.

19) G. Liu and M. Liu, *Smoothed Particle Hydrodynamics: A Meshfree Particle Method* (World Scientific Publishing, 2003).

20) M. Basa, N. J. Quinlan and M. Lastiwka, International J. Numerical Methods in Fluids **60** (2009), 1127.

21) G. K. Batchelor, *Introduction to Fluid Dynamics* (Cambridge University Press, New York, 1967).

22) A. Souto-Iglesias, L. Delorme, L. Pérez Rojas and S. Abril, Ocean Engineering **33** (2006), 11.

23) D. Molteni and A. Colagrossi, Comput. Phys. Commun. **180** (2009), 861.

24) S. Marrone, M. Antuono, A. Colagrossi, G. Colicchio, D. L. Touzé and G. Graziani, Comput. Methods Appl. Mech. Engrg. **200** (2011), 1526.

25) I. Fererico, S. Marrone, A. Colagrossi, F. Aristodemo and P. Veltri, *Proceedings* 5th *International Spheric Workshop, 22-25 June, Manchester, 2010*.

26) C. Wieselsberger, Physikalische Zeitschrift **23** (1922), 219.

27) R. Wille, Adv. Appl. Mech. **6** (1960), 273.

28) R. D. Henderson, Phys. Fluids **7** (1995), 2102.

29) H. Zhang, U. Fey and B. Noack, M. König and H. Eckelmann, Phys. Fluids **7** (1995), 779.

30) Y. T. Ng, C. Min and F. Gibou, J. Comput. Phys. **228** (2009), 8807.

31) Y. Lecointe and J. Piquet, Computer & Fluids **12** (1984), 225.

32) M. Braza, P. Chassaing and H. H. Minh, J. Fluid Mech. **165** (1986), 79.

33) C. H. K. Williamson, An. Rev. Fluids Mech. **28** (1996), 477.

34) A. Roshko, "On the development of turbulent wakes from vortex streets", NACA Rep. 1191 (1954).

35) L. Kovasznay, Proc. Roy. Soc. A **198** (1949), 174.

36) M. H. Wu, C. Y. Wen, R. H. Yen, M. C. Weng and A. B. Wang, J. Fluid Mech. **515** (2004), 233.